MissionDPT: Simulation and forecasting of radiation doses and health risks for space exploration missions

Shaowen Hu[1], Janet E. Barzilla[2], Diego Laramore[2], Marlon Núñez[3], and Edward Semones[4]

[1] KBR, Houston, TX, USA
[2] Space Exploration and Mission Operations, Leidos, Houston, TX, USA
[3] Department of Languages and Computer Sciences, Universidad de Málaga, 29016 Málaga, Spain
[4] Space Radiation Analysis Group, NASA Johnson Space Center, Houston, TX, USA

Abstract

Radiation exposure in space presents significant challenges to crew health and performance. To mitigate its impacts, research in space radiation environment, mass shielding geometry, nuclear interactions, transport codes and biological responses has been conducted for decades, offering many established models and codes. In this work, a web tool MissionDPT (Mission Dose Projection Tool) is reported which incorporates the most up-to-date version of these codes with simple input and output interface, enables interested users to calculate dose quantities and estimate acute risks for any low Earth orbits (LEO) and beyond LEO missions. Simulation results for dosimeters flown during the Artemis I and International Space Station (ISS) missions with known shielding files and trajectories are reasonably close to their measurements. A set of solar energetic particle forecasting models, University of Malaga Solar particle Event Predictor (UMASEP), are also integrated to provide dose information before or near the onset of solar particle events (SPEs). With archived Geostationary Operational Environmental Satellite (GOES) solar proton data from 1986 to present (real time data updated every 5 minutes), MissionDPT can be used either to analyze the radiation exposure and acute health risks for historical severe SPEs, or to serve as a console tool for flight operational team in contingent scenarios for the upcoming lunar and Mars missions.

Plain Language Summary

New advances in understanding the space radiation environment, physics, transport models, and biological responses have been made recently, offering many established models and codes to describe the radiation field and risks in space. A web tool MissionDPT (Mission Dose Projection Tool) is reported which incorporates the most up-to-date version of these codes with simple input and output interface, enables interested users to calculate dose quantities and estimate acute risks for various exploration missions. It also integrates the University of Malaga Solar particle Event Predictor (UMASEP) models to provide forecasting capability for dose and risk projection of solar particle events in real time or for historical cases.

Key Points:

- Quick calculation for dose quantities at a user selected cadence, allowing direct comparison with dosimeter measurements in real time or after the missions
- A library of SPEs spanning over 40 years (1986-present) with continuous GOES proton fluxes calibrated with other sources
- A flight console tool capable of nowcasting and forecasting dose quantities and risks in contingency scenarios

1. Introduction

Health risks associated with space radiation are recognized as one of the most significant challenges to human space exploration. These include latent effects such as carcinogenesis, cardiovascular disease, and central nervous system decrements, etc., and acute radiation syndrome (ARS) that may manifest during missions (Cucinotta et al., 2010). The particles of galactic cosmic rays (GCR) encompass a broad spectrum of highly penetrating particles covering elements up to Ni and beyond with energy up to 10^{13} MeV, inducing a continuous low dose rate background in space flights that is hard to reduce by conventional shielding strategies (Slaba et al., 2017). When approaching the Earth, these charged particles become trapped in Van Allen Belts (VAB) or South Atlantic Anomaly (SAA) because of the interactions with the Earth's magnetic field (Xapsos, 2019), in which the protons and electrons are the dominant species, with highest energies up to 1 GeV and 10 MeV, respectively. An additional source of space radiation comes from our Sun, which occasionally discharges large numbers of energetic particles that can populate significant parts of heliosphere for hours or even days (Reames, 1999). The large solar energetic particle (SEP) events can add significant radiation dose to astronauts in a short period of time and can induce acute clinical responses during the mission if no sufficient shielding is provided (Hu et al., 2009); however, the vehicle usually provides shielding for the lower energy particles.

The radiation environment for space missions is highly dependent upon the location of interest and solar activities. In low Earth orbit (LEO), the geomagnetic field deflects a portion of GCR and all but the most intense solar particle events (SPE), and the terrestrial shadow cast by the Earth also attenuates the intensity of the particles (Slaba et al., 2025). However, passing through SAA like the orbits of International Space Station (ISS) can elevate the dose rates several magnitudes higher (Zeitlin and Pinsky, 2020). The GCR intensity and SPE frequency are modulated by the heliosphere magnetic field on an ~11-year cycle, which can be characterized by the sunspot numbers (SSN) and the solar 10.7-cm radio flux (F10.7) (Xapsos, 2020). GCR intensities are anti-correlated with solar maximum and minimum, while the SPE frequency is opposite. The occurrence of SPE can also change the configuration of trapped protons and electrons (Xapsos, 2020). For interplanetary exploration beyond the Earth's protective magnetosphere such as the planned lunar and Mars missions, trapped particles are just briefly present; however, the intensities of GCR and SEP are higher than LEO missions as a recent study demonstrated

(Slaba et al., 2025). Near planetary surfaces such as the Earth, the Moon or Mars, the interactions of ambient deep space radiation environment with the surface and/or atmospheres can generate secondary particles, which further complicate the local radiation environment and modify the associated health risks (Norbury et al., 2020).

To characterize these complex radiation environments that astronauts may experience, researchers in the past decades have made significant advances in modeling the ambient space radiation environment, mass shielding geometry, and atomic and nuclear interaction parameters, and in developing fast and reliable radiation transport codes to estimate radiation dose quantities and various health risks (Norbury et al., 2020). Simulation results obtained through these computational tools are rather consistent with dosimetry measurements for vastly different scenarios and highly complex and diverse shielding configurations (George et al., 2024; Slaba et al., 2025). In this paper we describe a web tool MissionDPT (Mission Dose Projection Tool) which incorporates the most up-to-date version of space radiation environment models and transport code, with associated various physics and biological models, and show how it can be used to calculate dose quantities of interest and estimate acute risks for various missions in real time and with historical events. Simulation results will be compared with dosimetry measurements when data are available. This tool also utilizes a set of established SEP forecasting models which predict SEP integral intensities at different energy levels, to reconstruct differential spectra for transport calculation so as to provide dose information before or near the onset of an event either historically or in real time.

This paper is organized as follows: Section 2 describes the interface of MissionDPT, section 3 summarizes the workflow of the tool and various models and codes involved, section 4 showcases the modeling results of some missions with comparison of dosimetry measurements, section 5 describes and demonstrates the capability of SEP dose forecasting of the tool, and section 6 presents discussion and conclusions.

2. Interface of MissionDPT

Like its predecessors ARRT1.0 (Hu et al., 2020) and AART2.0 (Hu et al., 2025), MissionDPT is a webtool with all input parameters and output results displayed together in one webpage (Figure 1). The input panel includes data selection and parameter selection sections. The current version uses 2 datasets: Cal-GOES dataset which can be utilized to do mission simulation from 1986-01-01 to present, and UMASEP forecasting dataset (combination of GOES data and UMASEP model outputs) which can generate additional SEP forecasting dose information from 1997-01-01 to present. Both datasets are updated by retrieving data from NOAA National Centers for Environmental Information (NCEI) website (https://www.ngdc.noaa.gov/ngdc.html), as well as the ISWA – HAPI Server at NASA Goddard Space Flight Center (GSFC) (https://iswa.gsfc.nasa.gov/IswaSystemWebApp/hapi/), once daily and once every 5 minutes, respectively. After selecting a dataset, user can select an SPE of interest from the indicated drop box, which has a list of events based on years of studies of GOES

(Geostationary Operational Environmental Satellite) data. The event onset and background starting time are automatically displayed with a default 12-hour time window (Figure 1). All these parameters can be modified by users. The default data cadence is 5 minutes, but users can choose 60, 30, 15, 10, or 1 minutes. The results of 1 minute cadence can be generated to compare with ISS (International Space Station) and other missions dosimetry measurements, in agreement with the current active monitoring instrument suite.

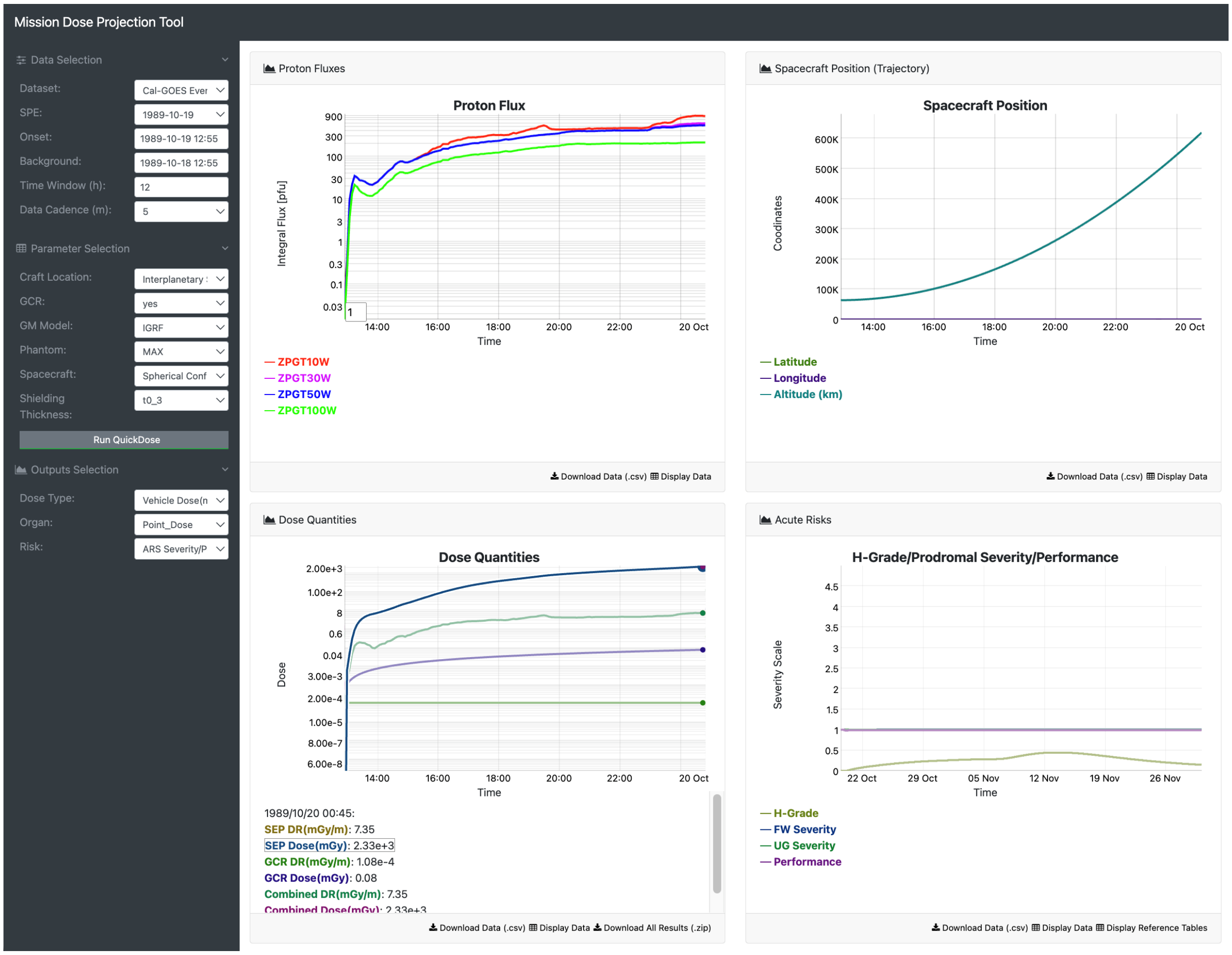

Figure 1. One-page web interface for MissionDPT.

The mission parameter selection starts with spacecraft location. Five options are currently available: interplanetary space, lunar surface, ISS, transit, and user supplied trajectory. For analysis after 1999-01-01, minutely ISS trajectories can be retrieved locally, which are archived by SRAG (Space Radiation Analysis Group) at NASA JSC (Johnson Space Center). For real time analysis, ISS trajectories are retrieved from "Spot the Station" website (https://www.nasa.gov/spot-the-station/). For analysis before 1999-01-01, a one-day ISS trajectory is used for rough calculation if user is interested in simulating the impacts to ISS of historical events. The transit trajectory is represented by the Artemis I trajectory (George et al., 2024), and the user supplied trajectory can be uploaded by preparing with the format in Figure 2 (top). Analysis for interplanetary space and lunar surface does not need specified trajectory, however, an illustrative plot is still generated in the spacecraft position for mission parameter sanity check (Figure 1).

```
data:
time_tag,Latitude,Longitude,Altitude (km)
2025-05-10 07:05:00,43.08154154423106,-152.41573186986778,421.14650417440157
2025-05-10 07:06:00,45.05438268246161,-148.01275831305293,421.35881183703293
2025-05-10 07:07:00,46.82432663943174,-143.29672227697247,421.8593363134885
```

```
10000 1
121 2.28854000e+01 0
121 6.62614000e+00 0
121 2.33311000e+01 0
```

Figure 2. Format for user supplied trajectory file (top) and user supplied shielding file (bottom).

The next option for mission parameter selection is to choose if additional source of radiation is of interest to analyze simultaneously. GCR can be chosen for Beyond LEO (BLEO) missions, and SEP can be selected for LEO missions. For LEO missions, 3 geomagnetic models can be selected to investigate the solar storm impacts to dose simulations, the international geomagnetic reference field (IGRF) (Alken et al., 2021) for quiet time, T96 (Tsyganenko, 1996) and TS05 (Tsyganenko and Sitnov, 2005) for storm time. Then 4 phantom types – CAM, CAF, MAX, FAX (Slaba et al., 2009) – can be selected for organ dose and health risk calculation. “No phantom” can also be selected to generate dose in silicon if user is only interested to compare with instrument measurements. The last 2 options for mission parameter selection are for shielding configuration for spacecraft. For aluminum spheric configuration, user can choose various thicknesses with unit g/cm^2 in the next drop box. For ISS, various shielding files can be selected to represent the shielding configurations of the onboard detectors (Zeitlin and Pinsky, 2020), which are developed by SRAG. For Orion MPCV (Multi-Purpose Crew Vehicle), options of shielding are available for 6 Hybrid Electronics Radiation Assessor (HERA) sensors, the 4 crew seat locations, and the 4 locations inside storage bays available in the storm shelter configuration. A user supplied shielding file can be uploaded by preparing with the format in Figure 2 bottom. Only lines starting with “121” and a space are parsed by the code of the tool, and the number of rays is not limited to be 10000. The current version of the tool is tested with 1 layer of aluminum and can be expanded to run with 2 layers of shielding with aluminum and polyethylene.

After making data selection and mission parameter selection, user can click the “Run QuickDose” button to submit the jobs to SRAG-managed cluster, which can be finished within minutes. The results are sent back to the web server and are plotted in the Dose Quantities and Acute Risks sections (Figure 1). Three types of dose quantities can be plotted: absorbed dose (mGy), Gray-Equivalent (mGy-Eq), and dose-equivalent (mSv). If a phantom model is selected, instrument point dose as well as BFO (blood forming organs) and skin doses can be displayed, and 2 types of acute risks (Figure 1, references in Hu et al. 2020) can be plotted. If no phantom model is selected, only point dose can be displayed, and no result is generated for acute risks. Figure 1 shows the selection of Cal-GOES data for the first 12 hours of the 1989-10-19 event with 5-minute cadence, a MAX phantom in a 0.3 g/cm^2 Al spherical vessel during interplanetary mission, the point dose quantities and the acute risks during the mission. Note the data at any point can be displayed by hovering mouse on the plots and can be retrieved by clicking the “Download Data” and “Display Data” links below the plots, and all results (risks and doses) can be downloaded in a zip file by clicking the “Download All Results” link below the dose quantities plot.

3. Components and workflow of MissionDPT

One component of MissionDPT that does not display in the interface is the differential proton fluxes/fluences, which are used to generate SPE spectrum for transport calculation. For analysis before 2020-01-01, the Cal-GOES differential fluxes of 5-minute cadence are used for both datasets, but the UMASEP forecasting dataset has additional UMASEP forecasting fluxes associated with SPEs, which will be described in following sections. The Cal-GOES is a continuous and uniform dataset of solar proton fluxes encompassing energies from 10 to 1000 MeV during the years of 1986-2019, which is derived from GOES 6-15 by calibrating with models of Ground Level Enhancement (GLE) events based on measurement of multiple satellites and ground neutron monitors (Hu & Semones, 2022a; 2022b).

To get the spectrum of the user-specified data cadence, one-day average fluxes at different energy levels are firstly calculated as background, which are then subtracted from the proton fluxes during the period of interest. If the total flux of the 4 highest energy channels is greater than 0.01 #/(cm^2 s sr MeV), a slope is calculated from them in log scale and is used to extrapolate the spectrum with power law to higher energy grids up to 2500 MeV (Hu et al., 2016). For energy grids between 10 and 1000 MeV, the fluences are calculated via interpolation, and the spectrum is cut off below 10 MeV as the protons at these energy levels are insignificant for dose calculation (Hu et al., 2025). Spectra of user-specified cadence > 5 minutes are obtained by summing the fluxes, while one-minute spectra are those 5-minute spectra divided by 5. For analysis between 2020-01-01 and 2025-04-01, GOES 16 fluxes are used, with calibrated energies based on the modeling of the 2017-09-10 event (Hu & Semones, 2022a). For analysis after 2025-04-01 and real time, GOES 18 fluxes are used at the writing of this report, assuming the same effective energies for different channels as GOES 16. The procedure to derive the spectrum of user-specified cadence is the same as from Cal-GOES dataset.

The NASA deterministic radiation transport code HZETRN2020 (High charge, Z, and Energy TRaNsport) (Wilson et al., 1991; 2014; Slaba et al., 2020), is utilized in this tool, with Badhwar-O’Neill (BON) 2020 as the default GCR model (Slaba & Whitman, 2020) and AP9 and AE9 as the default trapped proton and electron models, respectively (Ginet et al., 2013). While for interplanetary space full spectra for GCR and SEP are used, for lunar surface the corresponding spectra are cut to half because of the blockage of the Moon. Albedo particles produced by nuclear collisions between the incoming GCR ions and lunar regolith can contribute to effective dose varying between 1-32% (Slaba et al., 2011).

MissionDPT calculates a solar modulation factor ϕ based on the selected dates and applies it on a lunar albedo look-up table pre-computed by BON2020 to estimate the albedo doses due to GCR. SEP can also generate albedo particles but are less significant compared with GCR (Norbury et al., 2020) and their contribution is not considered in the current version.

For LEO environment such as the ISS trajectories, the GCR is also attenuated, due to the magnetosphere shielding and the terrestrial shadow cast by the Earth (Slaba et al., 2024). This is implemented in HZETRN2020 by coupling with the latest 14th International Geomagnetic Reference Field (IGRF) model (Alken et al., 2021). However, this internal geomagnetic field can be suppressed by the embedded magnetic field in the enhanced solar wind during intense solar particle events, which is not considered in HZETRN2020. We incorporated a publicly available COR code (https://github.com/COR-Cut-off-rigidity/) (Gakesek et al. 2022) in MissionDPT to include semi-physics-based external geomagnetic model T96 (Tsyganenko, 1996) and TS05 model (Tsyganenko & Sitnov, 2005) to simulate the geomagnetic storm effects. For LEO missions, users can select either IGRF, IGRF+T96, or IGRF+TS05 to check the impacts of geomagnetic storm to dose estimation (Mertens et al., 2024). Figure 3 illustrates that, during the 2024-05-11 Gannon Storm, the cutoff rigidities at some ISS trajectory points (close to highest latitudes) are extended to lower values with additional T96 and TS05 models.

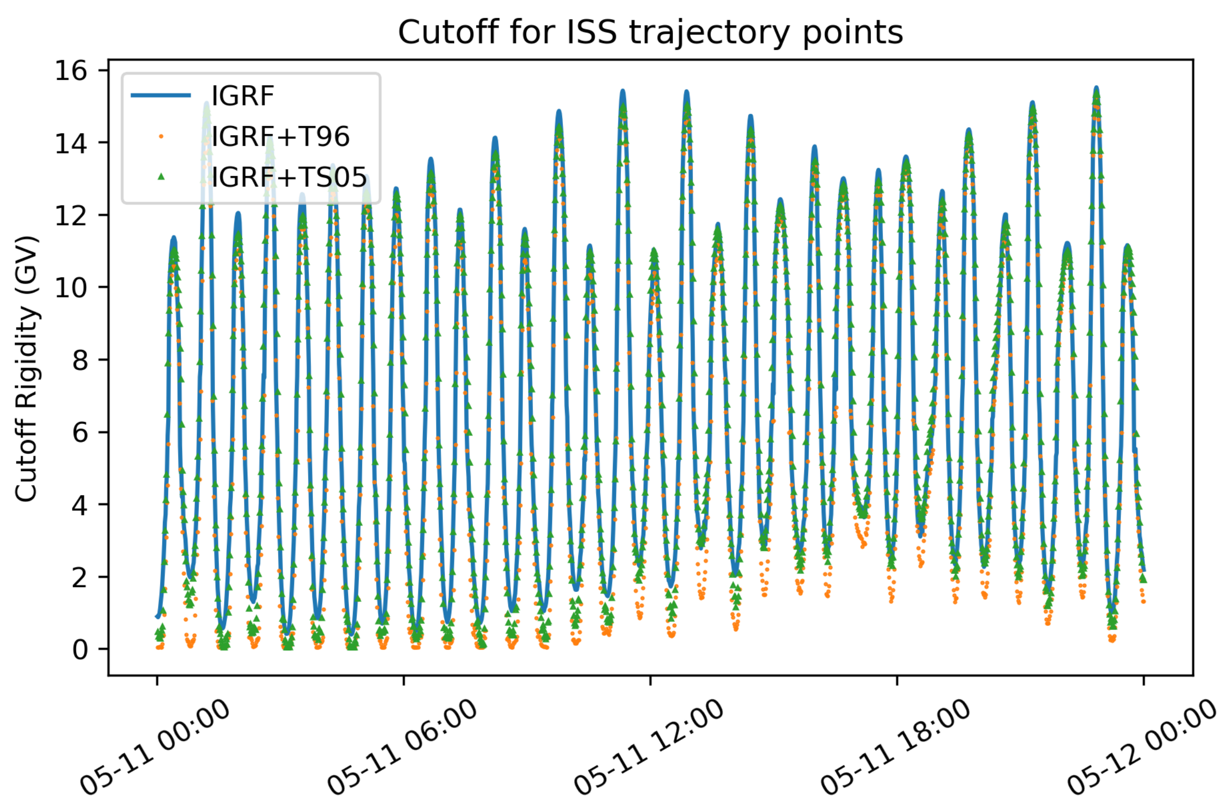

Figure 3. Vertical cutoff changes for ISS trajectory points during the 2024-05-11 Gannon Storm. The cutoff rigidities at some ISS trajectory points (close to highest latitudes) are

extended to lower values when external T96 and TS05 models are used, which are calculated with COR code (Gakesek et al., 2022).

To get transmission functions for trajectory points inside geomagnetic field, the vertical cutoffs need to be converted into directionally averaged cutoffs (Mertens et al., 2023). This is accomplished by the modified GEOFFB code in HZETRN2020. By substituting the subroutine to calculate vertical cutoff with the COR generated vertical cutoff value, the results of transmission function of 4 points and the truncated spectra of 3 particles at 2 points are shown in Figure 4. The terrestrial shadow (blockage) provided by the Earth can also be seen in this figure, indicating about 68% particles of free space can access the craft location if their rigidities are higher than the cutoffs. These results are consistent with previous report of HZETRN modeling on ISS trajectory at quiet time (Slaba et al., 2010). At storm time, the transmission functions will be pushed to lower rigidities and the spectra to lower energies, implicating more particle depositions and higher doses at the craft locations. These effects will be discussed in the following section. The same transmission function is used to get truncated SEP spectrum for SPE dose calculation (Section 4)

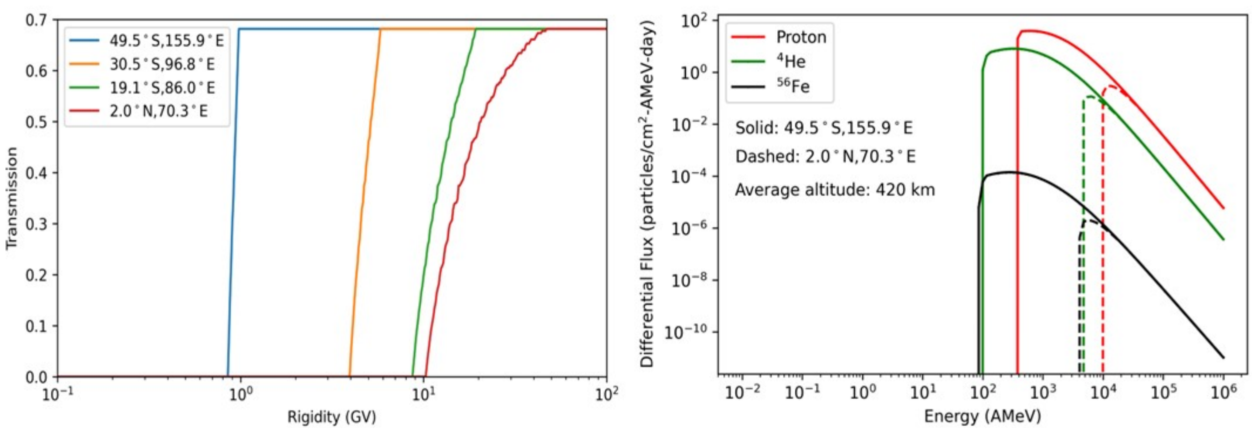

Figure 4. Quiet time transmission function of 4 points of ISS trajectory calculated from directionally averaged cutoffs (left), and truncated spectra of 3 particles at 2 points (right).

The engine of MissionDPT is a set of python scripts called "QuickDose", which takes inputs and submits jobs to run HZETRN codes in a repository provided by developers at NASA Langley Research Center (LaRC). QuickDose first obtains the boundary conditions for transport calculation based on user-selected mission location/trajectory and radiation sources, then manages parallel jobs of transport calculation with HZETRN code on the SRAG cluster to get dose quantities at spatial grids of aluminum, tissue or silicon, which include 3 types of doses, i.e., absorbed dose (Gy), Gray-Equivalent dose (Gy-Eq), and effective dose (Sv). 1 Gy is defined as the net absorption of 1 Joule of energy in 1 kilogram of any material (NCRP, 2000), Gy-Eq is defined as the dose in Gy multiplied by the RBE (relative biological effectiveness) for particle species and energy (Hu et al., 2009), while Sv is defined by multiplying absorbed dose in Gy with quality factors associated with specific types of radiation, either ICRP60's Q (ICRP, 1991) or NASA's Q (National Academies of

Sciences, Engineering, and Science, 2021; NASA, 2023). Organ doses and detector doses are then calculated by interpolating and summing through the organ thickness of the selected phantom model (Slaba et al., 2009) and the skin thickness of the spacecraft shielding file.

The last component of MissionDPT is a set of ARS models describing deterministic effects of severe SPEs, which include H-grade (HemoGrade), severity scale of UG (upper gastrointestinal) and FW (fatigue and weakness) symptoms, and PD (performance decrement), and the counts of lymphocytes, granulocytes, leukocytes, and platelets (Hu et al., 2020). Like in ARRT, the tool does not set a threshold for the ARS models but generates results of various endpoints whenever a phantom model is selected. However, these models are not triggered if no phantom model is selected.

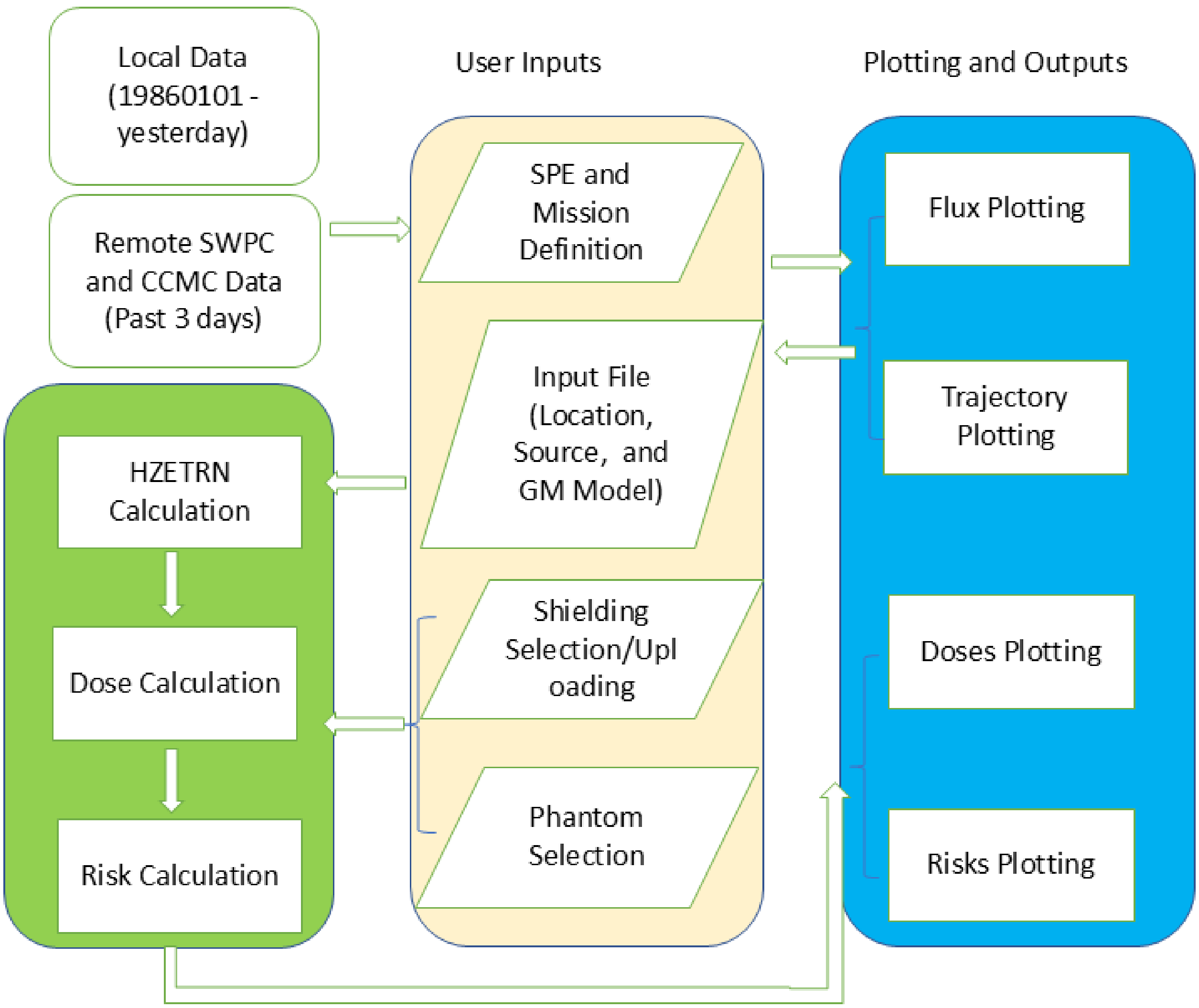

Figure 5. Workflow of MissionDPT. 2 types of data (historical and real time) are retrieved from other institutes, processed, and stored automatically. Items in “User Inputs” provide multiple choice to specify the mission and user-interested endpoints of transport calculations, where those in “Plotting and Outputs” are the 4 plots showing in the web

interface. The trajectory files, spectra files, as well as input files for transport calculations are sent to SRAG-managed cluster, where the 3 types of calculation are managed by QuickDose and run sequentially, and results are sent back to MissionDPT server for plotting and user retrieval.

The workflow of different modules of MissionDPT is illustrated in Figure 5. The local data are updated daily, prepared automatically for past event analysis, while real time data are updated every 5 minutes, all by “crontab” commands of python scripts managed to run on the webserver. After selecting/modifying SPE and mission parameters, integral proton flux and mission trajectory will be plotted, and an input file is generated including all options to run HZETRN code and dose calculation. When user clicks the “Run QuickDose” button, the input file, as well as the differential proton flux files and trajectory file are sent to SRAG-managed cluster, and parallel jobs are run on available nodes. The interface will receive an alert when all jobs are finished, indicating all relevant output files are sent to the webserver for dose quantities plotting (and risks plotting if a phantom model is selected). If the cluster is free, a calculation of 1440 points (one day’s data with 1 minute cadence) with phantom model and 10k rays of shielding thicknesses takes about 10 minutes.

4. Mission dose simulations

4.1 Artemis missions

If the trajectory of the mission and shielding configuration of the spacecraft are known, MissionDPT can perform simulations for LEO and BLEO missions no matter whether an SPE occurs. Next the results will be presented of the simulations for Artemis I/II and measurements for Artemis I. As our team (SRAG) has been closely working with these missions aiming to send US astronauts back to the lunar surface, detailed trajectory and shielding configurations of locations of interest in the Multi-Purpose Crew Vehicle (MPCV) Orion are available before each mission, and the measurements of the various onboard dosimeters can be downlinked for ground analysis in real time during the mission, MissionDPT can be used as a mission console tool like ARRT (Hu et al., 2020; 2022) to provide radiation doses and health risks information to the flight operations team in contingency scenarios.

For Artemis I, one set of Hybrid Electronic Radiation Assessor (HERA) detectors, comprised of three sensors (HPU, HSU1 and HSU2) were mounted at fixed locations in Orion (George et al., 2024). Figure 6a shows their measurements and simulated dose rates by MissionDPT from 7:00 to 8:30 UTC on 2022-11-16, during which the spacecraft passed the inner proton belt shortly after the launch (George et al., 2024). The time profiles of calculated dose rate elevating, reaching peak, and then declining to the background are quite consistent with measurements, indicating the AP9-IRENE model’s description of this region (Ginet et al., 2013) and the transport calculation are fairly accurate. The modelled total doses during this 40-minute outbound section are about 8.4 -15% less than the measurements, with discrepancy mainly contributed during the peak times, during which the simulated dose rates are about 70-80% of the recorded (Figure 6a) as reported before (George et al., 2024).

The lower dose rates of HPU and HSU2 than simulations shortly after the peak times can be well explained by the rotation of Orion lasting 5 minutes to execute trans-lunar injection (George et al., 2024). Such reductions were not observed in HSU1 (Figure 7), which was in the storm shelter of the stowage bays close to the heat shield and service module (Hu et al., 2020). Though the shielding configurations of HPU and HSU1 are similar (George et al., 2024), the local shielding of HSU1 might have prevented it from recording the variation of particles due to the spacecraft maneuver. These results demonstrate the sensitivity and reliability of these detectors developed for space radiation environment monitoring, as well as the state-of-the-art capability of the computational models embedded in MissionDPT to characterize the space radiation exposure.

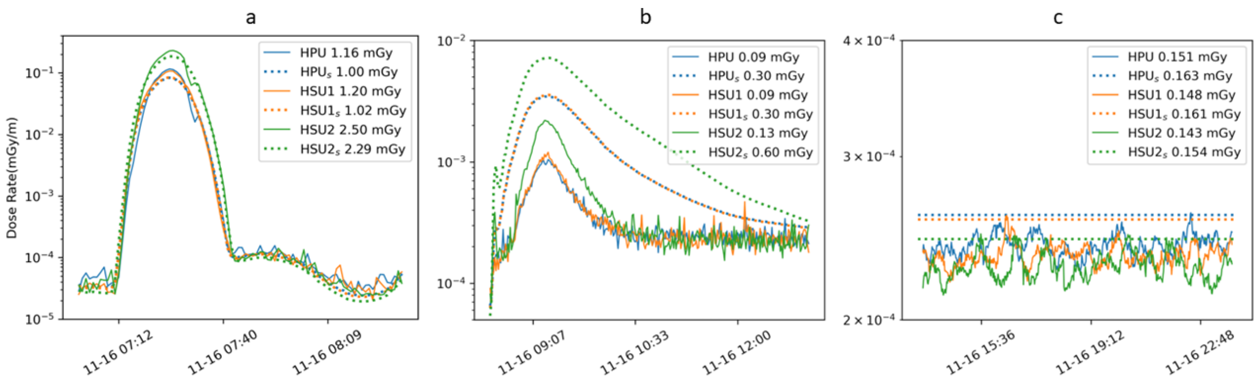

Figure 6. Measurements and simulations of the dose rates of HERA sensors during the inner proton belt pass (a), outer electron belt pass (b), and GCR only for the first day of the mission (c). (a) and (b) are minutely data, while (c) measurements are smoothed with 20 points for clarity. The legends also show the total Si doses for measurements (HPU, HSU1, and HSU2) and simulations by MissionDPT (HPU_s, $HSU1_s$, and $HSU2_s$) for the 3 sections.

From 8:45 to 10:45 UTC 2022-10-16, the spacecraft passed the outer electron-rich belt (George et al., 2024), and HERA sensors recorded elevated dose rates (Figure 6b) due to the emitted bremsstrahlung photons from the interactions of energetic electrons with the spacecraft material (Attix, 1986). The simulated dose rates for three sensors are significantly higher than the measurements, and the simulated elevation extends till 13:30 UTC (Figure 6b). This outer belt zone is known for its volatile and dynamic nature (Xapsos, 2020) and is challenging to model (Ginet et al., 2013), and the results of transport calculations for electrons with HZETRN code are not as good as those with Monte Carlo codes (Slaba et al., 2013). Though the results show the limitation of current computational models, as indicated by a previous study where the total doses for this section are negligible (≈ 1%) compared with the inner belt passage which comprised of 23% of the total mission dose (George et al., 2024).

After passing the outer belt, the spacecraft entered free space with only GCR contributing to radiation exposure for this mission (George et al., 2024). Figure 6c shows the measurements and simulations of the HERA sensors from 13:30 to 23:59 UTC on 2022-11-16. The simulated doses are about 7.9%, 8.8%, and 7.7% overestimated, respectively, with errors larger than HZETRN2020 3D mode calculations (Slaba et al., 2025). Compared with the SAA passage, the measurements of the 3 detectors are closer to each other, indicating the ineffectiveness of shielding to reduce the GCR exposure. Though with more shielding, HPU and HSU1 received increased exposures compared to HSU2, due to nuclear interactions and associated secondary radiation such as neutrons and pions (Slaba et al., 2025), which is also demonstrated by simulation results (Figure 6c). The simulations were run using the default ACE/CRIS oxygen flux to estimate modulation parameter ϕ (Slaba and Whitman, 2020). If the sunspot number (SSN) was used, the relative errors would be -13.9%, -13.5%, and -16.4%, respectively.

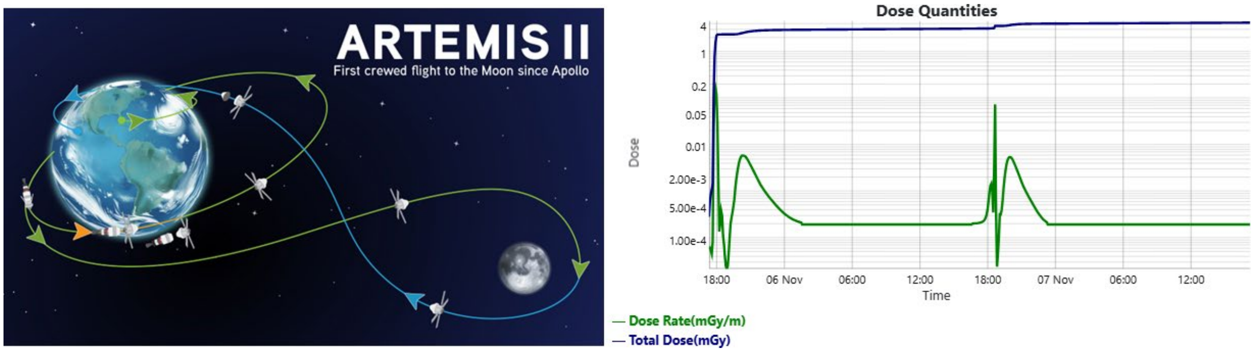

Figure 7. Schematic trajectory of MPCV Orion for Artemis II (left, from nasa.gov) and simulated dose quantities of HPU1 for the first 2 days (right) from MissionDPT.

Artemis II mission, the first crewed flight to the moon since Apollo, is scheduled to launch soon at the writing of this paper. Two sets of HERA units will be onboard at fixed locations for this 10-day mission, with schematic trajectory in Figure 7. Unlike Artemis I, the spacecraft will pass twice through the van Allen belts during the outbound section, according to the latest planned trajectory. The simulated dose rates of one sensor shown in Figure 7 indicate the exposure profile of the first pass will be like Artemis I, and the second pass will be shorter and lower, presumably due to higher speed and higher altitude. The simulated peak dose rate of the first pass is about 2 times that of the Artemis I (Figure 6a), but this may change as the trapped radiation models are dependent on the mission time (Ginet et al., 2013). After launch, with a more specific trajectory and more accurate shielding configuration, the simulated detector dose quantities can be used in mission operation tools such as ARRT (Hu et al., 2020; 2025) to compare with real-time measurements.

4.2 ISS dose measurement and modeling during SPEs

Dosimeters onboard ISS usually document excess radiation exposure during severe SPEs at specific points at high latitudes along the trajectory, where the Earth's magnetic field is not strong enough to deflect all highly energetic particles. Geomagnetic storms accompanying such events can further weaken the field and allow more energetic particles to impact the instruments onboard ISS. Next the results are discussed for MissionDPT's simulations for ISS-RAD during the 2024-05-10 Gannon event, with comparison of the dose quantities modeled with the quiet time geomagnetic model IGRF14 and storm time model TS05 with the instrument measurements. Induced by a series of solar flares and coronal mass ejections (CMEs) toward Earth, the Gannon event started at 2025-05-10 13:40 UTC, with >100 MeV proton fluxes crossing the 1 pfu (particle flux unit, i.e., proton/(cm^2 s sr)) threshold on 05-11 02:05 until 23:35 that day (Figure 8 (left)). Meanwhile, the solar storm K_p index rose to > 7 after 05-10 15:00 and maintained at that level the whole following day (Figure 8 (right)), providing a perfect opportunity to investigate the SEP impacts to LEO missions such as ISS.

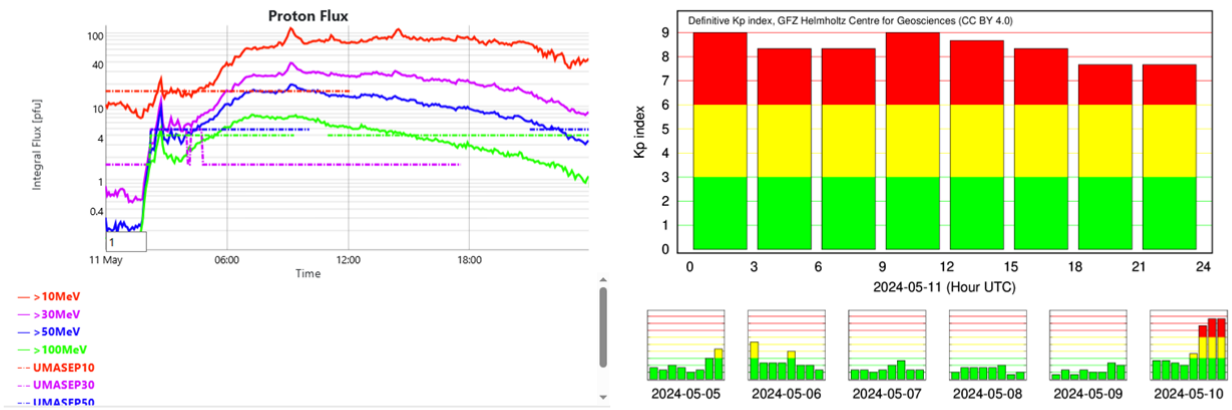

Figure 8. Integral proton fluxes and UMASEP predictions of the 2024-05-11 event (Generated with MissionDPT) (left) and Kp index during and before the event (Generated from GFZ Helmholtz Centre for Geosciences at https://kp.gfz.de/en/) (right).

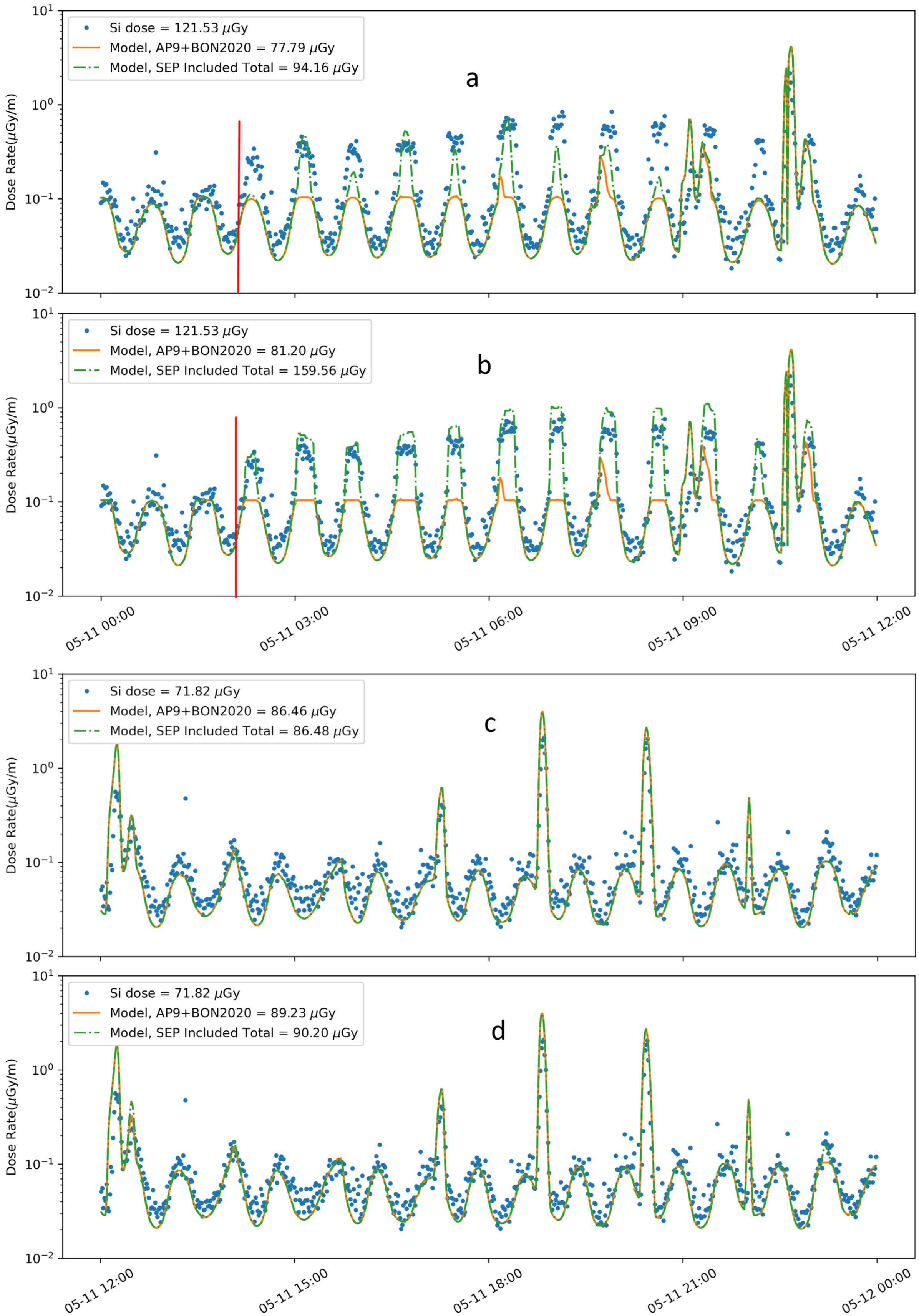
Si dose = 121.53 μGy
Model, AP9+BON2020 = 77.79 μGy
Model, SEP Included Total = 94.16 μGy
a
Si dose = 121.53 μGy
Model, AP9+BON2020 = 81.20 μGy
Model, SEP Included Total = 159.56 μGy
b
Si dose = 71.82 μGy
Model, AP9+BON2020 = 86.46 μGy
Model, SEP Included Total = 86.48 μGy
c
Si dose = 71.82 μGy
Model, AP9+BON2020 = 89.23 μGy
Model, SEP Included Total = 90.20 μGy
d
Dose Rate(μGy/m)
05-11 00:00
05-11 03:00
05-11 06:00
05-11 09:00
05-11 12:00
05-11 15:00
05-11 18:00
05-11 21:00
05-12 00:00

Figure 9. ISS-RAD measurements for the first half day (top 2) and the second half day (bottom 2) of the 2024-05-11 event and MissionDPT simulations with IGRF14 geomagnetic model only (a and c) and with IGRF14+TS05 models (b and d). The red vertical lines in (a) and (b) indicate the onset of the event (2024-05-11 02:05 UTC) (Figure 8).

Figure 9 shows the ISS-RAD measurements during 2024-05-11, along with MissionDPT simulations, with IGRF14 geomagnetic model only (a and c), and with IGRF14+TS05 models (b and d). ISS-RAD is a dosimeter resembling the Radiation Assessment Detector (RAD) for the Mars Science Laboratory Curiosity Mars rover (Hassler et al., 2012), deployed in various modules of ISS since 2016 (Zeitlin & Pinsky, 2020). As the ISS orbits the earth every 90 minutes, in an orbit with an inclination of 51.6° and an altitude of about 420 km, the RAD measurements exhibit a sinusoid pattern due to variations of the geomagnetic field strength (weak at high latitudes and strong at low latitudes) to block GCRs, with additional spikes due to the trapped particles while ISS passes SAA several times each day (Figure 9). We broke the measurements and simulations into two halves as in the second half day the contributions of SEP are nearly negligible (Figure 9 c and d), and the total dose ISS-RAD recorded for the first half day is about 50 μGy (≈69%) higher than the second half. Though the intensity of proton fluxes and storm index Kp of the two halves are at the same levels (Figure 8), the cutoff rigidities of the second half of the ISS trajectory of that day are significantly higher than the first half, no matter if the storm models T96 or TS05 are included or not (Figure 3). At most positions with high latitude of first half day trajectory, the additional storm models T96 and TS05 push the cutoff rigidities to nearly zero (Figure 3), allowing particles at all energy levels reaching the spacecraft and inducing enhanced measurements inside the station.

Using quiet time geomagnetic model IGRF14, the simulated total dose for ISS-RAD for the first half day is underestimated by about 27 μGy (Figure 9a). The dosimeter recorded the enhancement due to SEP shortly after the onset (02:05 UTC), but the simulations miss it (Figure 9a). The simulated enhancements are close to measurements for the second, fourth, and sixth high latitude passes from onset, but are significantly underestimated for the others (Figure 9a). With storm model TS05 added, all enhancements simulated during high latitude passes since onset are comparable to measurements, though overestimated for some (Figure 9b). It is interesting to note the simulated dose rate profiles by IGRF14+TS05 during the passes have plateaus resembling measurements (Figure 9b), i.e., they do not continuously increase to a peak and then decrease from it, such as the simulated profiles by IGRF14 only (Figure 9a). This can be explained by the cutoff rigidity extension by the storm models discussed above. With cutoff rigidities push to nearly zero, though particles at all energy levels are allowed to penetrate the geomagnetic field to reach the spacecraft, low energy particles cannot get through the skin of the spacecraft for lacking sufficient penetration power. On the contrary, the lowest cutoff by IGRF14 of that day is about 0.411 GV (≈ 85.63 MeV) and the rigidity shapes are sharp during the high latitude passes (Figure 3), so the simulated dose rate profiles by IGRF14 have sharp peaks rather than plateaus (Figure 9a). Though closer to the dose rate profile of measurements, the IGRF14+TS05 simulated total dose is 38 μGy higher for the first half day, indicating further improvements are still needed for these models. IGFR14+T96 results are even higher as the cutoff rigidities are pushed lower than TS05 (Figure 3), so they are not discussed in this report.

For the second half day, the simulations with IGRF14 generate total dose nearly the same as that of AP9+BON2020 (Figure 9c), while those with IGRF14+TS05 add about 1 μGy (Figure 9d), i.e., the SEP contribution is negligible. Though the energetic proton (> 100 MeV) fluxes were still above the threshold (Figure 8 left), the cutoff rigidities at highest latitudes are high enough for the geomagnetic field to block them to reach the spacecraft (Figure 8 right), as discussed above. The storm model increases 2.77 μGy for GCR exposure, close to the 3.41 μGy for the first half day. The differences of AP9+BON2020 between Figure 9a and 9b and between 9c and 9d are attributed to GCR only as the AP9 model applied is independent of the geomagnetic models. For the second half day, the combined total doses of AP9 and BON2020 are about 15 and 18 μGy higher than the measurements (Figure 9c and 9d). These overestimations apparently come from AP9 model simulations, as the modeled peaks for all SAA passes are significantly higher than the instrument measurements (Figure 9c and 9d). Simulations for the first half day also show such overestimations, though the number of times passing SAA are fewer (Figure 9a and 9b). It is known the occurrence of SPE can change the configuration of trapped protons and electrons (Xapsos, 2020); these results implicate more sophisticated model is needed to estimate more accurately their contribution to radiation exposure.

5. SEP dose forecasting

5.1 UMASEP models

UMASEP is a set of SPE prediction tools forecasting the occurrence and integral proton fluxes at different energy levels, including UMASEP10, UMASEP30, UMASEP50, UMASEP100, and UMASEP500 (Núñez, 2011; 2015; 2022). Each tool includes a well-connected and a poorly-connected prediction model, the former makes use of the lag-correlation of solar electromagnetic flux with the particle flux from GOES measurements, while the latter checks whether the differential proton flux behavior is similar to that in the beginning phases of previous historically events and thus deduce similar consequences (Núñez, 2011; 2015). Recently, each model also launches machine-learning-based predictions of the SEP integral proton intensity and fluence for a specific energy bin (Núñez, 2020). UMASEP10 and UMASEP100 were validated with data from January 1994 to September 2013, obtaining Probability of Detection (POD) of all >10 MEV and >100 MeV SEP events of 88.6%, 80.85%, False Alarm Ratio (FAR) of 23.24%, 29.62%, and average warning time ≈4 h, ≈1 h, respectively (Núñez, 2015). Since 2010, NASA's integrated Space Weather Analysis system (iSWA) and the European Space Weather Portal have redistributed UMASEP forecasts, obtaining successful results on an operational level (Hu et al., 2025).

5.2 Fluence model update

For each UMASEP model, a fluence model was derived based on the proton flux/fluence correlation formula obtained from SEPEM data set (Whitman and Núñez, private communications), which was developed by calibrating GOES 5-15 proton fluxes with NASA IMP-8/Goddard medium energy (GME) experiment data set (Sandberg et al., 2014). A recent study indicated the calibrated energies of P6 and P7 channels of GOES 8-15 are underestimated, causing the rendered fluence spectrum softer for SEP and underestimated radiation dose through transport calculation (Hu & Semones, 2022a). The Cal-GOES data set developed by calibrating GOES 6-16 proton data with GLE modeling remedied such caveats (Hu & Semones, 2022) and was applied to update the fluence models described as following.

47 events during 1997-2013 reported in Núñez, M. (2015) were selected to identify the correlation formula between integral proton fluxes and differential fluences at energy levels corresponding to UMASEP10, UMASEP30, UMASEP50, and UMASEP100. The starting time (ST) of an event was determined by examining the flux >100 MeV when it exceeds 1 pfu (the onset of ESPE (Energetic Solar Particle Event), and fluxes F>10 (ST+7h), F>30 (ST+6h), F>50 (ST+5h) and F>100 (ST+3h) are point fluxes at the specific time after the onset of each event, obtained from data of GOES 8, 11, and 15 during this period. These fluxes are those the 4 UMASEP models predict if forecasts are issued. To get the differential fluence, an in-house software WASPE (Web App for Solar Particle Events) was used to obtain background-subtracted fluxes from the Cal-GOES data first (Hu & Semones, 2022a; 2022b), then the 7 hours' fluxes from the onset of the event were added with cadence factor (5 min). The reason to use the fluences at 4 energy levels (Figure 10) of 7 hours uniformly rather than model specific (as for integral fluxes) is for the purpose of dose projection, with which the predicted spectrum can be used to give dose information a bit further in time.

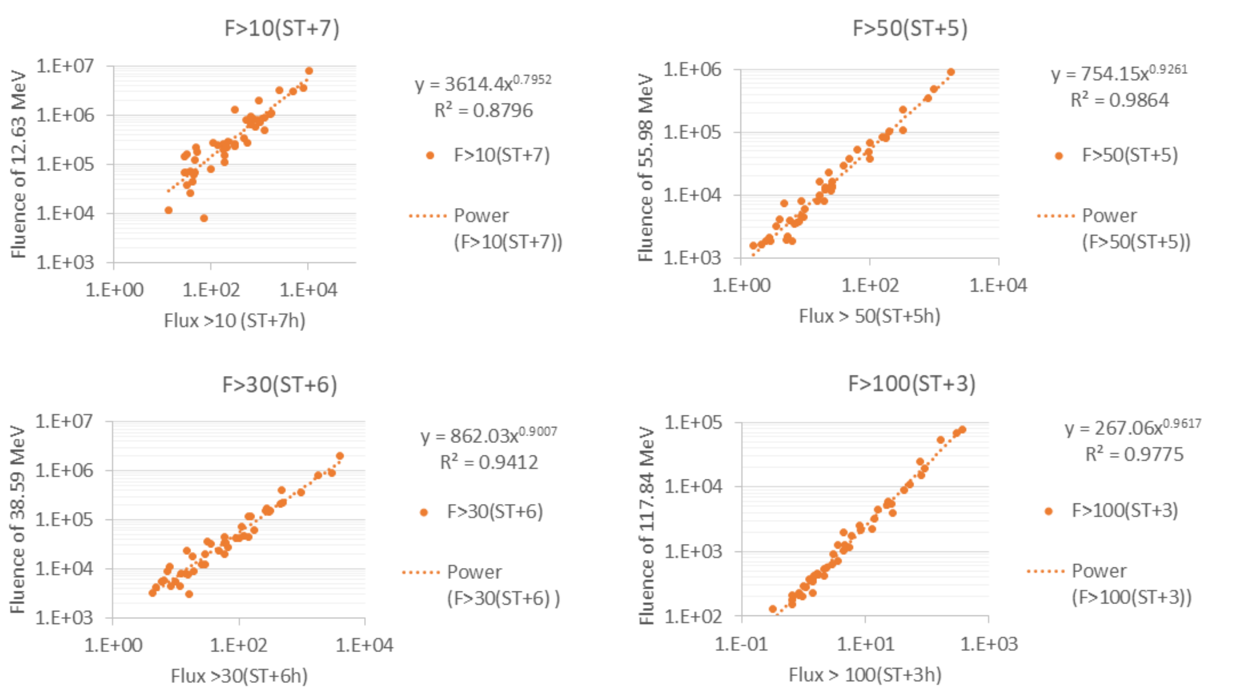

Figure 10. Correlation formula of integral proton flux and differential fluence at 4 energy levels for the 47 events during 1997-2013.

The correlation formual between the integral fluxes and the differential fluences of the 47 events at 4 energy levels were identified with the power law fitting of MS Excel chart tool (Figure 10). The R^2 values in the figure indicate the correlation at each energy level is high enough to lay the groundwork to utilize UMASEP forecasting for dose projection. Note UMASEP500 was not utilized in current version, as too few historical events are available to identify a reliable correlation formula.

5.3 Spectrum fitting

The predicted spectrum needs to extrapolate to higher energies, as previous studies found that proton fluxes with energies greater than hundreds MeV are the most relevant to the absorbed doses for detectors/crew inside typical spacecrafts such as MPCV (Hu et al., 2020; 2025). Three functional forms were investigated with the same 47 events during 1997-2013, and the Band function was identified as the best to fit UMASEP predicted spectrum, for all cases if forecasts at 3 and 4 energy levels are available, and most cases if 2 energy levels forecasts are made (Appendix). The Band function fittings with 2 predictions at >10 MeV and >30 MeV as well as at >10 MeV and > 50 MeV involve large uncertainty, and the forecasting dose information for them will not be reliable and need to be interpreted with caution.

We managed to run UMASEP models for the events during 1997-2017, including the 47 events reported in Núñez, M. (2015) and the 2017-09-10 event. For each of these events the UMASEP forecasts were generated from one day before the onset to the end of the event. From 2021-01-01 to present, all the UMASEP forecasted results, as well as real time forecastings, are retrieved from the ISWA – HAPI Server at NASA Goddard Space Flight Center (GSFC) (https://iswa.gsfc.nasa.gov/IswaSystemWebApp/hapi/). When an event is selected from the list, the forecasted fluxes are compiled with the GOES integral proton fluxes and plotted together (Figure 8). An algorithm was developed to check if forecasts are just the repetitions of those previous, if the forecasts are made at least 2 energy levels, and if the flux values are monotonically decreasing with increasing energies. Only the first set (>2) of monotonically decreasing fluxes is applied with the correlation formula to get fluences and is then fitted with Band function to render a spectrum. For most events, only a few such spectra are generated, as the UMASEP models are intended to forecast proton fluxes at specific time rather than their time profiles (Núñez, 2015).

5.4 SPE dose projection

Each first forecasted spectrum is used to do transport calculation to get the dose rate for the specified time point. For the 2024-05-10 Cannon event, such spectra were generated at 05-10 18:10, 05-11 2:00, 2:15, 10:10, 11:00, and 21:00 (Figure 11a). Because the fluences are projected to be of 7 hours, the dose rates are then multiplied by 7 hours to get the forecasted total dose of 7 hours since the time point. While the projected dose rate and total dose of the last time point are extended to 7 hours later, each of those before it is also extended till new spectra is generated (Figure 11b).

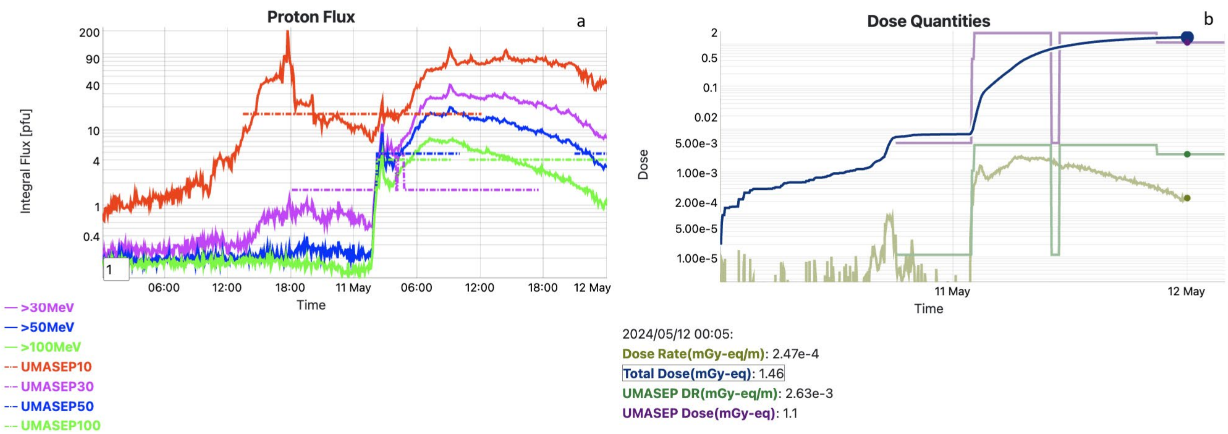

Figure 11. UMASEP forecasting of the 2025-11-10 event (a) and dose projection with MissionDPT (b).

Figure 11b shows the BFO dose quantities calculated for FAX model at Seat 1 in Orion MPCV in free space for the event. During the period with proton > 100 MeV flux < 1 pfu (before 5-11 2:05), the combination of UMASEP10 and UMASEP30 projected by MissionDPT a total dose 4.85 μGy-eq, lower than the calculated 11.80 μGy-eq from GOES data due to UMASEP10's underestimation (Figure 11). UMASEP100 issued a prediction at 5-11 2:00 (5 minutes before the ESPE onset), and the projected dose raised to 45 μGy-eq. At 2:15, the UMASEP100 proton flux forecasting changed from 1.63 pfu to 16.26 pfu, and UMASEP30 and UMASEP50 also issued predictions. With 4 model predictions together, the projected dose by MissionDPT changed to 1820 μGy-eq. Though higher than the total dose 670 μGy-eq for the following 7 hours, it is close to the total dose 1460 μGy-eq when the event approached the end (Figure 11b).

Though UMASEP30 issued predictions along with UMASEP50 and UMASEP100 for this event, the forecasted flux intensities were the same to one of them in the beginning of ESPE and dropped lower later (Figure 11a). As they did not meet the monotonic requirement, they were not used to get the fitted spectrum. However, both UMASEP50 and UMASEP100 stopped to issue prediction from 5-11 10:10 to 10:55, and UMASEP 30 predictions were utilized by MissionDPT together with UMASEP10 predictions to generate a much lower dose for that period (Figure 11b). After this drop, the combination of UMASEP10 and UMASEP100 predictions projected a same total dose as before the drop (Figure 11b). The later slight drop occurred at 5-11 21:00 was projected with combination of UMASEP50 and UMASEP100, indicating a difference between different combinations of model predictions.

5.5 Dose projections for historical events

Combining multiple UMASEP models for a forecasted spectrum, MissionDPT extends previous effort to utilize just UMASEP100 forecasting for mission dose projection (Hu et al., 2025). The forecasted spectrum can be used to get dose information for either free space, lunar surface, or LEO missions, if other required parameters such as shielding configuration, trajectory, etc., for transport calculation are available. To check the capability of UMASEP enabled dose forecasting, MissionDPT was applied to calculate the dose quantities for 47 events during 1997-2013 (Núñez, 2015), and 8 events during 2017-2025 (Table 1), to compare with UMASEP forecasted doses.

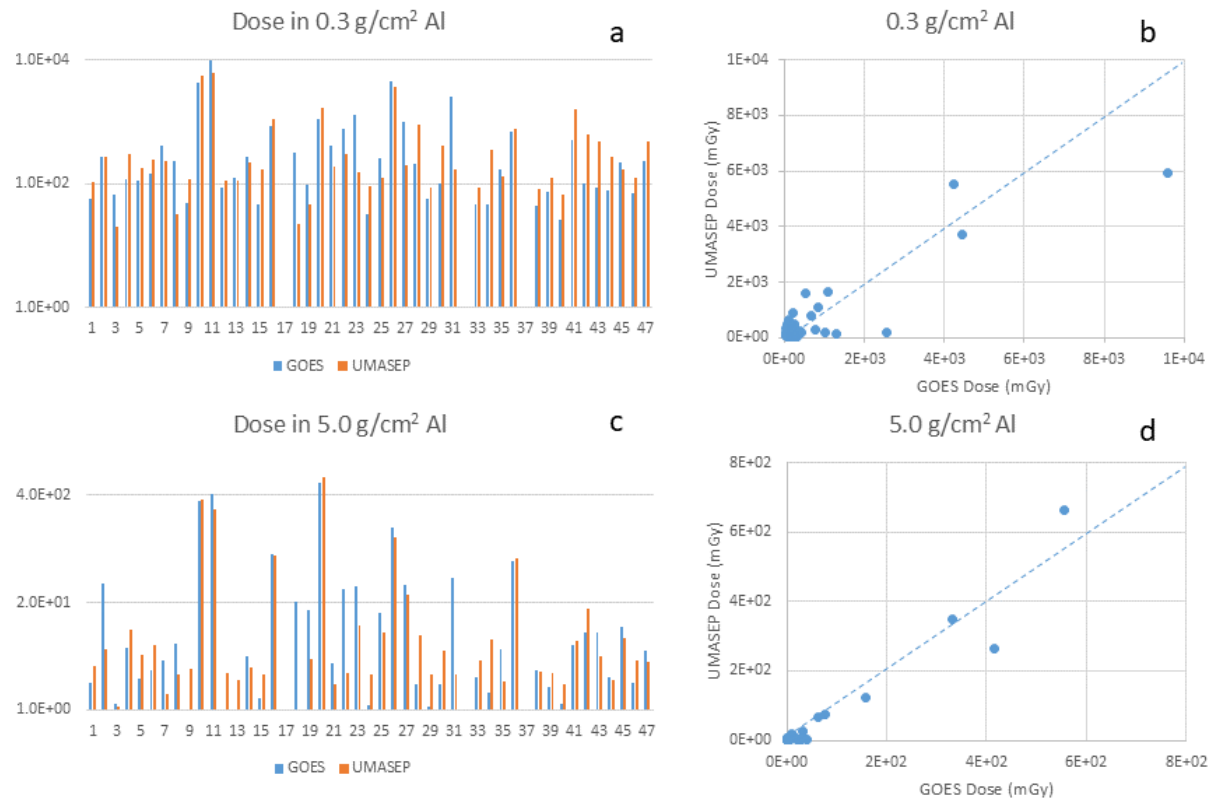

Figure 12. Comparisons between UMASEP projected Si doses and the 7-hour doses calculated from GOES data for the 47 events during 1997-2013, in 0.3 g/cm2 (a and b) and 5.0 g/cm2 (c and d) Al sphere in free space. Comparisons in log scale are in a and c, and in linear scale are in b and d (with 1:1 ratio lines to assist visualization).

Figure 12 shows the comparisons of the calculated Si doses of the first 7 hours from the onset of 47 events during 1997-2013, with UMASEP forecasted doses. With multiple model predictions combined, the number of missed events reduced from 6 events if only UMASEP100 is used (Hu et al., 2025) to 3 events (Figure 12 a and c). For thin shielding spacecraft (0.3 g/cm^2 Al), the numbers of events with overestimated and underestimated forecasting doses are comparable (Figure12 a and b). For spacecraft with more shielding (5.0 g/cm^2 Al), the forecasted first 7-hour doses of most events are underestimated, but are closer to the calculated values, especially for the 5 largest events (Figure 12 c and d). With more hit events, the averaged warning time (AWT) for the events during this period also increases from 59 minutes (Hu et al., 2025) to 84 minutes. These results indicate some improvement from previous effort of using UMASEP100.

Event Onset	UMASEP Issue Time	Warning Time
2017 09/10 16:20	16:15	5
2021 10/28 16:35	17:40	-65
2024 05/11 02:05	2:00	5
2024 06/08 02:25	2:55	-30
2024 07/23 02:05	2:30	-25
2024 10/09 03:50	3:15	45
2024 11/21 18:45	18:50	-5
2025 11/11 10:20	10:30	-10
AWT		-10

Table 1. Warning time of combining multiple UMASEP models for the 8 events during 2017-2025. Warning times are reported in minutes, and the last row reports the averaged warning time (AWT).

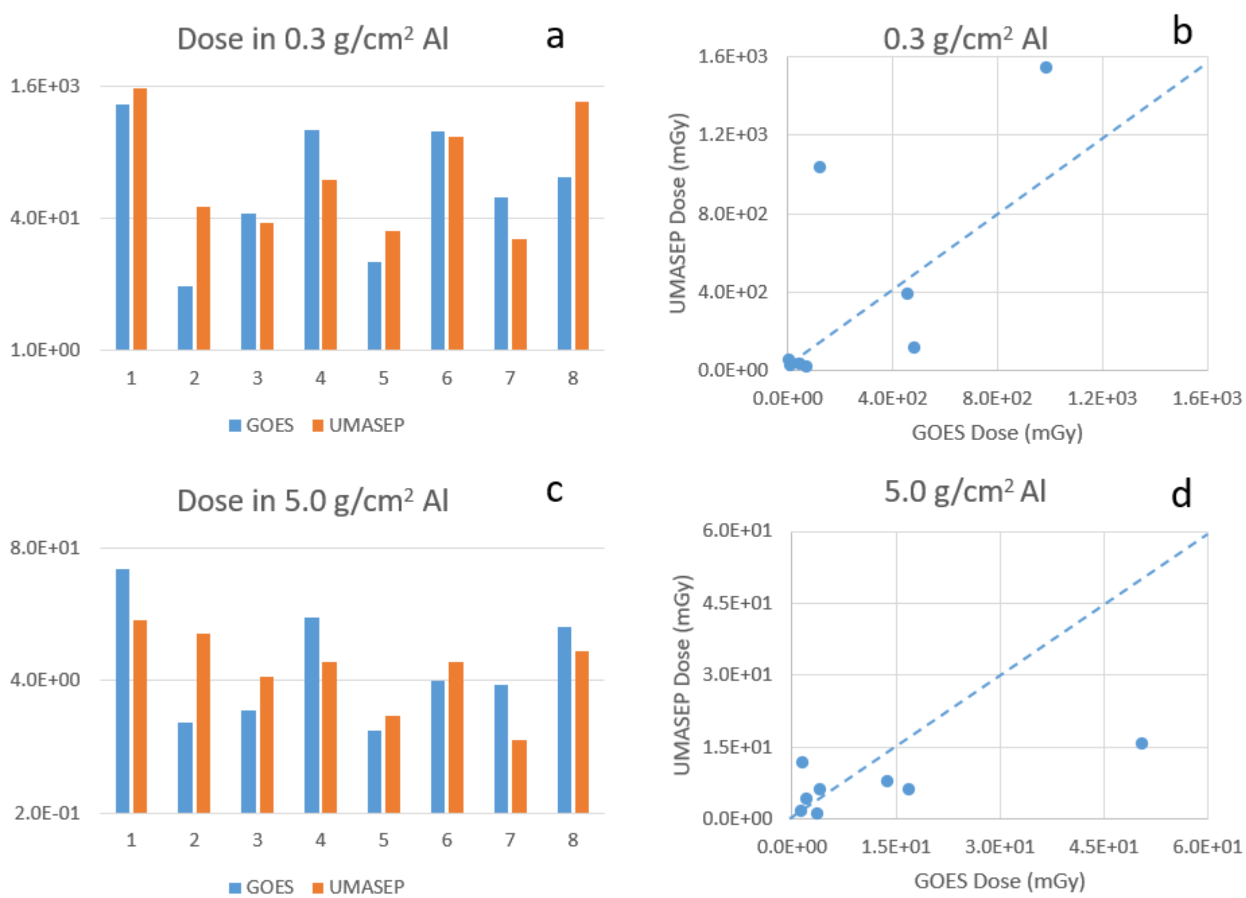

Figure 13. Comparisons between UMASEP projected Si doses and the 7-hour doses calculated from GOES data for the 8 events during 2017-2025, in 0.3 g/cm^2 (a and b) and

5.0 g/cm^2 (c and d) Al sphere in free space. Comparisons in log scale are in a and c, and in linear scale are in b and d (with 1:1 ratio lines to assist visualization).

After the 2017-09-17 event, only 7 ESPEs were recorded by GOES. Table 1 lists their onset times, UMASEP issue times, and the differences – the warning times. The forecasts were conducted by different versions of UMASEP models in real time at the CCMC (Community Coordinated Modeling Center) of GSFC (https://ccmc.gsfc.nasa.gov/models/UMASEP~v3/). 5 of the 7 events have negative warning times, with the largest delay of 65 minutes (Table 1). Figure 13 shows the forecasted doses for some over-estimated events within thin shielded spacecraft also became under-estimated for thicker shielding, but with larger discrepancies than the events in previous period. These results indicate the real time UMASEP forecasting needs further improvement, especially for models at high energies. To get a good estimation of dose information of large SPEs for operational purpose, the multiple UMASEP models still need to work together with other SPE forecasting tools (Whitman et al., 2022).

6. Discussion and conclusions

MissionDPT is a web tool incorporated the most up-to-date version of various space radiation environment models and HZETRN transport code, with associated multiple physical and biological models, and can be used to calculate dose quantities of interest and estimate acute risks for LEO and BLEO missions in real time and for historical events. Simulation results for dosimeters of the Artemis I mission and ISS with known shielding files and trajectories are reasonably close to their measurements, indicating significant advances achieved in decades of research and model development to characterize the complex radiation exposure and risks for space explorations. A set of UMASEP forecasting models were also integrated to provide dose information before or near the onset of SPEs. With archived GOES solar proton data from 1986 to present (real time data updated every 5 minutes), MissionDPT can be used either to analyze the radiation exposure and acute health risks for historical severe SPEs, or to serve as a console tool for flight operational team in contingency scenarios for the upcoming lunar and Mars missions.

MissionDPT is like NASA developed web tools OLTARIS (Singleterry et al., 2011) and NAIRAS (Mertens et al., 2010, 2012, 2013), all allowing engineers and scientists to run complete radiation analyses for exploration missions without being an expert in the various codes and models (Norbury et al., 2020). One advantage of MissionDPT is that quick results can be obtained for dose rates of a user selected cadence, particularly minutely dose rates that can be compared with dosimeter measurements in real time or after the missions. The direct comparison can greatly help validation and calibration for various models and codes, as the case studies in the work demonstrated. Another useful feature of MissionDPT is the continuous Cal-GOES dataset spanning over 40 years (1986-present) provides a library of SPEs with proton data consistent with other sources (Hu and Semones, 2022a), enabling user to do analyses and compare various strategies to mitigate exposure and risk of severe SPEs for specific missions. Additionally, the forecasting capability of MissionDPT is a bit more advanced than the recently published UMASEP-NAIRAS (Mertens et al., 2026), as the forecasted proton spectrum of this new module is dependent upon GOES proton flux of highest energy, while in this work the spectrum is independent of GOES measurements, therefore dose information could be given before the onset of an event. Like OLTARIS (Norbury et al., 2020), the framework of MissionDPT is modular and new models and methods can be added as they become available. Both tools are based on the most up-to-date version of the HZETRN code with the associated nuclear physics models, so MissionDPT can be useful for inter-code comparison and validation.

The current version of MissionDPT lacks real time geomagnetic modelling capability as the modeling parameters are retrieved from OmniWeb (https://omniweb.gsfc.nasa.gov/) and Dr. N. A. Tsyganenko's website (https://geo.phys.spbu.ru/~tsyganenko/TS05_data_and_stuff/), respectively, both do not update in real time. Efforts can be made to retrieve solar wind parameters from NOAA SWPC Data Service (https://services.swpc.noaa.gov/text/) or NESDIS Space Weather Portal (https://www.ncei.noaa.gov/cloud-access/space-weather-portal) if real time modelling for LEO missions is demanding. Another limitation is that the forecasting models UMASEP depend on the GOES measurements, restricting applications to earth bound missions only. As a recent study indicated the solar radiation environment of lunar is close to LEO (Zeitlin et al., 2025), the current Artemis missions can still utilize them. But for future Mars missions with most trajectories beyond the Sun-Earth line, onboard detectors measuring solar particle fluxes as well as X-ray intensities are necessary for forecasting and nowcasting dose projection with MissionDPT. One such system currently under development shows promising results in beamline testing and will be investigated in spaceflight applications (George et al., 2025). For Mars surface, secondary particles can be modelled for GCR and SEP to interact with its atmosphere and soil, which can expand the dose projection capability of Mission DPT. If the modeling of the interaction of energetic particles with the Earth's atmosphere can be implemented, MissionDPT can also be utilized to simulate aircraft radiation exposure like NAIRAS.

Acknowledgement:

This work was supported by NASA Human Health and Performance Contract NNJ15HK11B and Human Health and Performance Contract 2 (HHPC2). The authors appreciate Dr. Serkan Golke (NASA JSC) for sharing code to process parallel computing jobs on SRAG-managed cluster and are grateful to Dr. Stuart George and Dr. Thomas Campbell-Ricketts (NASA JSC) for sharing dosimeter data for Artemis-I and ISS missions. The application of geomagnetic storm models was benefited from stimulating discussions with Dr. A. Steve Johnson (NASA JSC), Dr. Tony Slaba and Dr. Christopher Mertens (NASA LaRC), we thank them for those discussions.

References:

Alken, P., Thébault, E., Beggan, C.D. et al. (2021). International Geomagnetic Reference Field: the thirteenth generation. *Earth Planets Space* 73, 49 doi: 10.1186/s40623-020-01288-x

Attix, F. H. (1986). Introduction to radiological physics and radiation dosimetry. John Wiley & Sons. https://doi.org/10.1002/9783527617135

Cucinotta, F.A., Hu, S., Schwadron, N.A., Kozarev, K., Townsend, L. W., Kim, M.-H. Y. (2010). Space radiation risk limits and Earth-Moon-Mars environmental models. Space Weather 8: S00E09.https://doi.org/10.1029/2010SW000572.

Gecášek, D., Bobík, P., Genči, J., Villim, J., Vaško, M., (2022). COR system: A tool to evaluate cosmic ray trajectories in the Earth's magnetosphere, Advances in Space Research, 70(4), 1153-1168, https://doi.org/10.1016/j.asr.2022.06.001.

George, S. P., Gaza, R., Matthiä, D. *et al.* (2024). Space radiation measurements during the Artemis I lunar mission. Nature 634, 48–52. https://doi.org/10.1038/s41586-024-07927-7

George, S.P., Campbell-Ricketts, T., Semones, E., Beavers, J., Umansky, P., Rozhdestvenskyy, S., Kroupa, M., (2025, July 6-10) The compact electron proton spectrometer - space weather nowcasting with a CdTe timepix2 based instrument [Conference presentation abstract]. 26th International Workshop on Radiation Imaging Detectors, Bratislava, Slovakia. https://indico.cern.ch/event/1428808/book-of-abstracts.pdf

Ginet, G. P., O'Brien, T. P., Huston, S. L. *et al.* (2013). AE9, AP9 and SPM: new models for specifying the trapped energetic particle and space plasma environment. *Space Sci Rev* **179**, 579–615. https://doi.org/10.1007/s11214-013-9964-y

Hassler, D. M., Zeitlin, C., Wimmer-Schweingruber, R. F., Böttcher, S., Martin, C., Andrews, J., et al. (2012). The Radiation Assessment Detector (RAD) investigation. *Space Science Reviews*, *170*(1–4), 503–558. https://doi.org/10.1007/s11214-012-9866-2

Hu, S., Barzilla, J. E., Núñez, M. & Semones, E. (2025). Real-time dose prediction for Artemis missions. J. Space Weather Space Clim. 15, 1. https://doi.org/10.1051/swsc/2024037.

Hu, S., Kim, M.-H. Y., McClellan, G. E., & Cucinotta, F. A. (2009). Modeling the acute health effects of astronauts from exposure to large solar particle events. *Health Physics*, *96*(4), 1–12.

Hu, S., Monadjemi, S., Barzilla, J. E., Semones, E. (2020). ARRT development for the upcoming human exploration missions. Space Weather 18: e2020SW002586. https://doi.org/10.1029/ 2020SW002586.

Hu, S., Semones, E. (2022a). Calibration of the GOES 6–16 high-energy proton detectors based on modelling of ground level enhancement energy spectra. J Space Weather Space Clim 12: 5. https://doi.org/10.1051/swsc/2022003.

Hu, S., Semones, E. (2022b). Multi-source calibrated GOES dataset and solar radiation environment model update. NASA/TP-20220008181. https://ntrs.nasa.gov/citations/20220008181.

International Commission on Radiological Protection. (1991). 1990 Recommendations of the International Commission on Radiological Protection (ICRP Publication 60). Annals of the ICRP, 21(1–3). Pergamon Press.

Mertens, C. J., Gronoff, G. P., Phoenix, D. B., Núñez, M., & Zheng, Y. (2026). Forecasting SEP atmospheric and space radiation by coupling UMASEP and NAIRAS models. Space Weather, 24, e2025SW004746. https://doi.org/10.1029/2025SW004746

Mertens, C. J., Gronoff, G. P., Zheng, Y., Petrenko, M., Buhler, J., Phoenix, D., Willis, E., Jun, I., and Minow, J. (2024). Commercial Crew Program (CCP) Post-flight Reference Radiation Environments, NASA/TM−20240012670, NESC-RP-19-01468: https://ccmc.gsfc.nasa.gov/publicData/models/NAIRAS/NAIRAS_TM_2024.pdf

Mertens, C. J., Gronoff, G. P., Zheng, Y., Petrenko, M., Buhler, J., Phoenix, D., Willis, E., Jun, I., and Minow, J. (2023). NAIRAS model run-on-request service at CCMC. *Space Weather*, 21, e2023SW003473. https://doi.org/10.1029/2023SW003473

Mertens, C. J., Kress, B. T., Wiltberger, M., Blattnig, S. R., Slaba, T. C., Solomon, S. C., Engel, M., (2010). Geomagnetic influence on aircraft radiation exposure during a solar energetic particle event in October 2003. Space Weather 8, S03006.

Mertens, C. J., Kress, B. T., Wiltberger, M., Tobiska, W. K., Grajewski, B., Xu, X., (2012). Atmospheric ionizing radiation from galactic and solar cosmic rays. Current Topics in Ionizing Radiation Research, edited by Mitsuru Nenoi, InTech Publisher, Rijeka, Croatia.

Mertens, C. J., Meier, M. M., Brown, S., Norman, R. B., Xu, X., (2013). NAIRAS aircraft radiation model development, dose climatology, and initial validation. Space Weather 11, 1-33.

National Academies of Sciences, Engineering, and Medicine. (2021). Space radiation and astronaut health: Managing and communicating cancer risks. The National Academies Press. https://doi.org/10.17226/26155

National Aeronautics and Space Administration. (2023). NASA spaceflight human-system standard: Volume 1, Crew health (NASA-STD-3001, Vol. 1, Rev. C). https://standards.nasa.gov/standard/NASA/NASA-STD-3001_VOL_1.

National Council on Radiation Protection and Measurements. (2000). Radiation protection guidance for activities in low-Earth orbit (NCRP Report No. 132). Bethesda, MD. https://ncrponline.org/shop/reports/report-no-132-radiation-protection-guidance-for-activities-in-low-earth-orbit-2000

Norbury, J. W., Slaba, T. C., Aghara, S., Badavi, F. F., Blattnig, S. R., Clowdsley, M. S., Heilbronn, L. H., Lee, K., Maung, K. M., Mertens, C. J., Miller, J., Norman, R. B., Sandridge, C. A., Singleterry, R., Sobolevsky, N., Spangler, J. L., Townsend, L. W., Werneth, C. M., Whitman, K., Wilson, J. W., Xu, S. X., & Zeitlin, C. (2019). Advances in space radiation physics and transport at NASA. Life Sciences in Space Research, 22, 98–124. https://doi.org/10.1016/j.lssr.2019.07.003

Núñez, M. (2011). Predicting solar energetic proton events (E > 10 MeV). Space Weather 9: S07003. https://doi.org/10.1029/2010SW000640.

Núñez, M. (2015). Real-time prediction of the occurrence and intensity of the first hours of >100 MeV solar energetic proton events. Space Weather 13: 807–819. https://doi.org/10.1002/2015SW001256.

Núñez, M. (2022). Evaluation of the UMASEP-10 version 2 tool for predicting all >10 MeV SEP events of solar cycles 22, 23 and 24. Universe 8: 35. https://doi.org/10.3390/universe8010035.

Núñez, M., Reyes-Santiago, P. J., Malandraki, O. E. (2017). Real-time prediction of the occurrence of GLE events. Space Weather 15: 861–873. https://doi.org/10.1002/2017SW001605.

Reames, D. V. (1999). Particle acceleration at the Sun and in the heliosphere. *Space Science Reviews*, *90*, 413–491.

Sandberg, I, Jiggens, P., Heynderickx, D., Daglis, I. A. (2014). Cross calibration of NOAA GOES solar proton detectors using corrected NASA IMP-8/GME data. Geophys. Res. Lett. 41: 4435–4441. doi:10.1002/2014GL060469.

Singleterry, R. C., Jr., Blattnig, S. R., Clowdsley, M. S., Qualls, G. D., Sandridge, C. A., Simonsen, L. C., et al. (2011). OLTARIS: On-line tool for the assessment of radiation in space. *Acta Astronautica*, *68*(7–8), 1086–1097. https://doi.org/10.1016/j.actaastro.2010.09.022

Slaba, T. C., Bahadori, A. A., Reddell, B. D., Singleterry, R. C., Clowdsley, M. S., & Blattnig, S. R. (2017). Optimal shielding thickness for galactic cosmic ray environments. Life Sciences in Space Research, 12, 1–15. https://doi.org/10.1016/j.lssr.2016.12.003

Slaba, T. C., Blattnig, S. R., Badavi, F. F., Stoffle, N. N., Rutledge, R. D., Lee, K. T., Zapp, E. N., Dachev, T. P., & Tomov, B. T. (2011). Statistical validation of HZETRN as a function of vertical cutoff rigidity using ISS measurements. Advances in Space Research, 47(4), 600–610. https://doi.org/10.1016/j.asr.2010.10.021

Slaba, T. C., Blattnig, S. R., Clowdsley, M. S. (2011). Variation in lunar neutron dose estimates, Radiation Research 176 (6), 827-841.

Slaba, T. C., Blattnig, S. R., Reddell, B., Bahadori, A., Norman, R. B., & Badavi, F. F. (2013). Pion and electromagnetic contribution to dose: Comparisons of HZETRN to Monte Carlo results and ISS data. *Advances in Space Research*, *52*(1), 62–78. https://doi.org/10.1016/j.asr.2013.03.009

Slaba, T. C., Qualls, G. D., Clowdsley, M. S., Blattnig, S. R., Walker, S. A., & Simonsen, L. C. (2009). Analysis of mass averaged tissue doses in CAM, CAF, MAX, and FAX (NASA/TP-2009-215562). NASA Langley Research Center. https://ntrs.nasa.gov/api/citations/20090017673/downloads/20090017673.pdf

Slaba, T. C., Rahmanian, S., George, S. *et al.* (2025). Validated space radiation exposure predictions from earth to mars during Artemis-I. npj Microgravity **11**, 6 https://doi.org/10.1038/s41526-025-00459-y

Slaba, T. C., Whitman, K. (2020). The Badhwar-O'Neill 2020 model. Space Weather 18, e2020SW002456

Slaba, T. C., Wilson, J. W., Werneth, C. M. & Whitman, K. (2020). Updated deterministic radiation transport for future deep space missions. Life Sci. Space Res. 27, 6–18

Tsyganenko, N. A., (1996). Effects of the solar wind conditions in the global magnetospheric configurations as deduced from data-based field models. In: International conference on substorms, vol. 389, p. 181.

Tsyganenko, N., Sitnov, M., (2005). Modeling the dynamics of the inner magnetosphere during strong geomagnetic storms. J. Geophys. Res. Space Phys. 110 (A3), A03208. https://doi.org/10.1029/2004JA010798.
Whitman, K., Egeland, R., Richardson, I. G., Allison, C., Quinn, P., et al. (2022). Review of solar energetic particle prediction models. Adv Space Res 72(12): 5161–5242. https://doi.org/10.1016/j.asr.2022.08.006.
Wilson, J. W., Slaba, T. C., Badavi, F. F., Reddell, B. D. & Bahadori, A. A. (2014). Advances in NASA radiation transport research: 3DHZETRN. Life Sci. Space Res. 2, 6–22
Wilson, J. W., Townsend, L. W., Schimmerling, W., Bhadhuri, J. E., Khan, F., Badhwar, G. D., Cucinotta, F. A., Shinn, J. L., Lamkin, D. L., & Miller, J. (1991). Transport methods and interactions for space radiations (NASA Reference Publication 1257). National Aeronautics and Space Administration, Langley Research Center. https://ntrs.nasa.gov/api/citations/19920006738/downloads/19920006738.pdf
Xapsos, M.A. (2019). A brief history of space climatology: from the big bang to the present. IEEE Transactions on Nuclear Science, vol. 66, no. 1, pp. 17-37, doi:10.1109/TNS.2018.2885649.
Zeitlin, C., Johnson, A. S., Schwadron, N. A., Spence, H. E., Wilson, J., Case, A. W., et al. (2025). Comparison of solar energetic particle flux measurements by CRaTER and GOES. Space Weather, 23, e2025SW004367. https://doi.org/10.1029/2025SW004367
Zeitlin, C., Pinsky, L. (2020). Current active detectors for dosimetry and spectrometry on the International Space Station. NASA Johnson Space Center. https://three.jsc.nasa.gov/Articles/CurrentActiveDetectors.pdf

Appendix. Spectrum fitting with UMASEP forecasted fluences

The spectra of SPEs are used to estimate radiation exposure to astronauts in space, either in the integral format or differential format. Historically, various analytical functional forms have been applied to fit the satellite data. Due to the limited energy resolution capability of particle detectors in early "Space Age era", the exponential in particle rigidity fitting method [Malitson and Webber, 1963] has been used in scientific community for several decades. The mathematical expression for the integral energy spectrum is:

$$\Phi(>E) = N_0 \exp\left(-\frac{R}{R_0}\right) \quad (1)$$

where Φ (>E) is the integral energy fluence in protons/cm2, N0 is a normalization constant, R is the proton rigidity (proton momentum) in MV (million volts), and R0 is the characteristic rigidity in MV. The proton rigidity R is related to the proton energy (MeV) by:

$$R(MV) = \sqrt{E^2 - 2m_0 E} \quad (2)$$

where E is the proton energy (MeV) and m0 is the rest mass of the proton (938 MeV) [Atwell et al., 2011]. In literature of SPE modeling, the exponential spectrum is usually extrapolated to the range of 10 MeV to several GeV. A similar scheme of spectrum modeling is using a Weibull function of the following form:

$$\Phi(> \mathrm{E}) = \Phi_0 \exp\left(-kE^{\alpha}\right) \quad (3)$$

where parameters Φ0, k, and α are determined by a nonlinear regression fit to the energy spectrum of interest [Xapsos et al., 2000]. A number of SPEs have been analyzed using this approach with maximum energy of 1 GeV [Kim et al., 2009].

A Band functional form of spectrum is getting more attention recently, which is a power law that rolls smoothly into a second, steeper power law, with a functional form that is continuous in both its value and derivative:

$$\begin{aligned}\Phi(> \mathrm{R}) &= \Phi_0 R^{-\gamma_1} \exp\left(-\frac{R}{R_0}\right), R \leq (\gamma_2 - \gamma_1)R_0 \\ &= \Phi_0 R^{-\gamma_2}\left\{[(\gamma_2 - \gamma_1)R_0]^{(\gamma_2-\gamma_1)} \exp(\gamma_2 - \gamma_1)\right\}, R > (\gamma_2 - \gamma_1)R_0 \quad (4)\end{aligned}$$

where γ1 and γ2 are respectively the spectral indices for the lower and higher energy branches. Parameters for the lower energy branch are obtained from satellite data from medium (10-100 MeV) and high (several hundred MeV) proton energies (GOES MEPAD and HEPAD and other satellites), while those for the higher energy branch are from cascade secondary neutrons produced during nuclear collisions of the incoming solar protons with the Earth's atmosphere (> 1 GV) [Tylka and Dietrich, 2009].

The above 3 functional forms were applied to fit the fluences UMASEP can forecast for the 47 events during 1997-2013 (Núñez, M., 2015), to test which form performs the best to extrapolate the spectrum to higher energies and to treat cases if one or two predictions are missing. Using the WASPE tool, 7-hour fluences of each event since onset were obtained with subtraction of the pre-event background fluxes, at energy levels of 12.63, 38.59, 55.98, 117.84, 170.98, 248.08, 359.59, 522.26, 747.75, 1100.00 MeV. The curve_fit module of scipy.optimze was used for each function, with 4, 3, or 2 fluences of the lowest energies as inputs to get the fitting parameters. The fitted function is then applied to the higher energies to get modeled fluences, and a Chi-Square formula $\chi^2 = \Sigma\, [(\text{Observed - Modeled})/\text{Observed}]^2$ is used to get the goodness-of-fitting R_chisq and an average $\bar{R}$ for 47 events. Figure A1 shows the schematic fitting with 3 functional forms, and the R_chisq of them for the 47 events and the average $\bar{R}$s if UMASEP predictions at 4 energy levels are available, indicating the Band function performs the best among them.

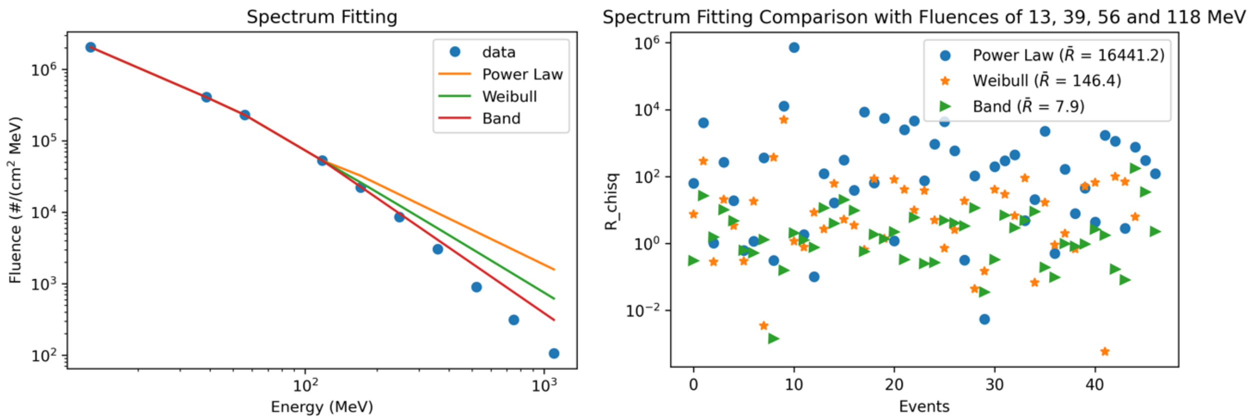

Figure A1. Schematic fitting with 3 functional forms, and the R_chisq of them for the 47 events and the average $\bar{R}$s.

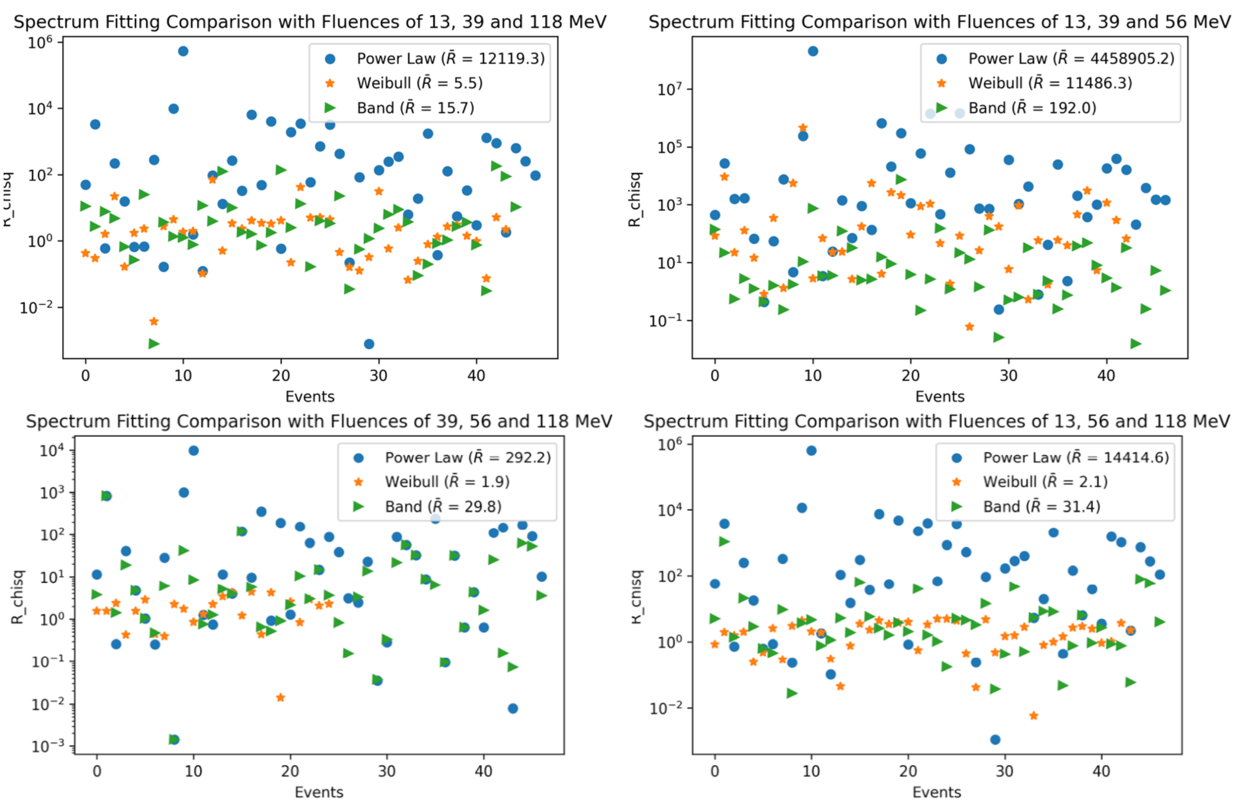

Figure A2. R_chisq of 3 functional fitting for the 47 events and the average $\bar{R}$s.

If one UMASEP prediction is missing, Weibull function fitting is better than Band function for some cases (Figure A2). However, for the predictions at 39, 56 and 118 MeV, Weibull fitting failed nearly half of the events (Figure A2, bottom left). Considering this, Band function is still the best among the 3 forms, its low average $\bar{R}$s indicating its goodness of fitting for all cases.

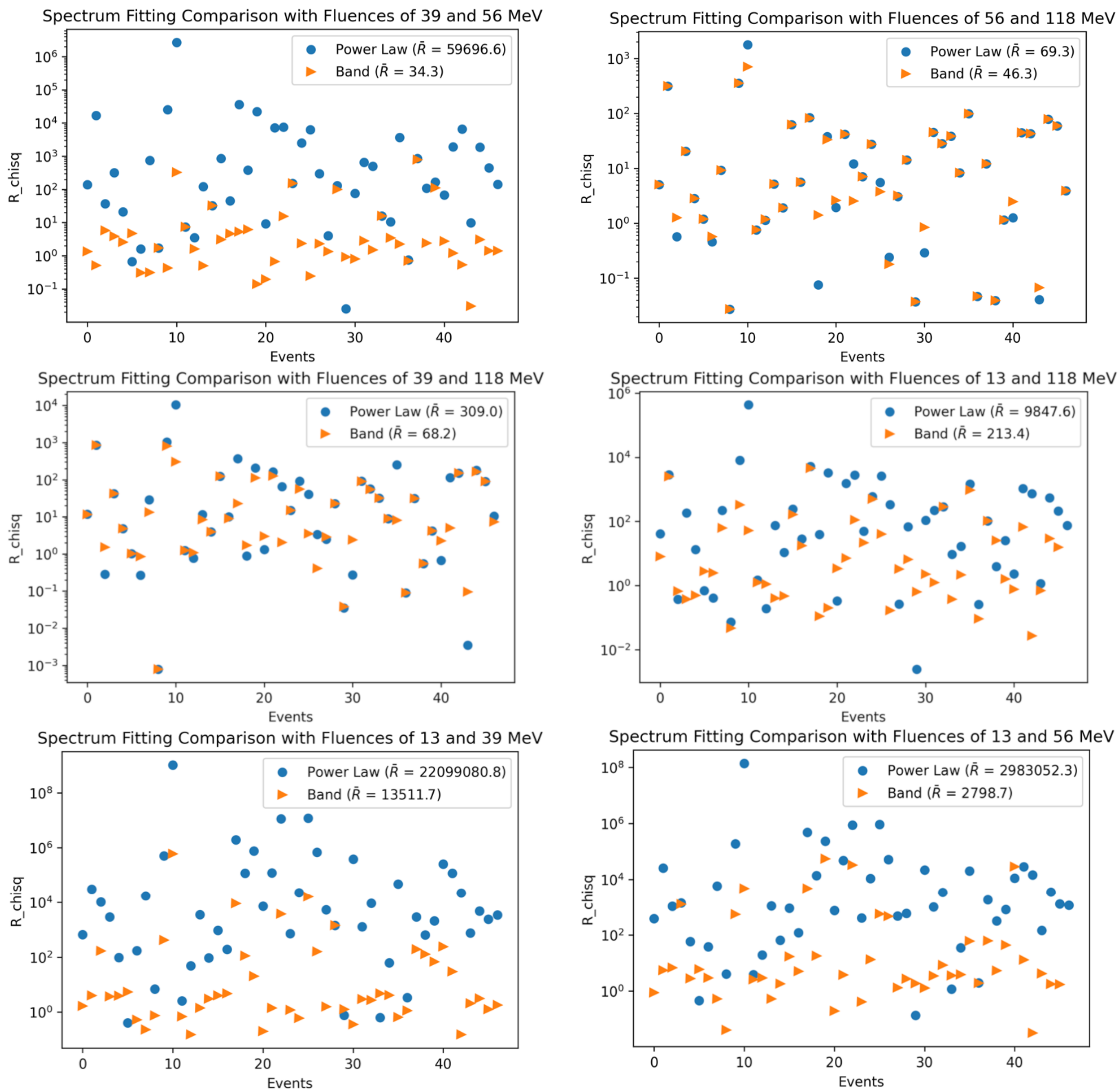

Figure A3. R_chisq of 2 functional fitting for the 47 events and the average $\bar{R}$s.

If only 2 UMASEP predictions are made, the Weibull functional form is unable to get any fitting parameters, while Band functional form can still get reasonable estimations of the fluences at higher energies, except for 2 cases, i.e., if the predictions are 13 and 39 MeV as well as 13 and 56 MeV (Figure A3).

Based on this investigation, Band function can be used to fit UMASEP predicted spectrum, with forecasting at 2, 3, or 4 energy levels, but fittings with 2 predictions at >10 MeV and >30 MeV as well as at >10 MeV and > 50 MeV have large uncertainty, and the forecasting dose information for them will not be reliable.

References:

Atwell, W., Tylka, A., Dietrich, W., Badavi, F., Rojdev, K. (2011). Spectral analyses and radiation exposures from several ground-level enhancement (GLE) solar proton events: a comparison of methodologies, presented at 41st International Conference on Environmental Systems, International Conference on Environmental Systems (ICES), Portland, Oregon, July 17-21

Kim, M-H. Y., Hayat, M. J., Feiveson, A. H., and Cucinotta, F. A. (2009). Prediction of frequency and exposure level of solar particle events, Health Physics, 97, 68-81.

Malitson, H. H. and Webber W. R. (1963). A summary of solar cosmic ray events, in The Solar Proton Manual, NASA TR R-169, Washington D. C.

Tylka, A. J. and Dietrich W. F. (2009). A new and comprehensive analysis of proton spectra in ground-level enhanced (GLE) solar particle events, Proceedings of the 31st International Cosmic Ray Conference, Lodz, Poland, Universal Academy Press.